Monthly Notices of the ROYAL ASTRONOMICAL SOCIETY

MNRAS **548,** 1–33 (2026) https://doi.org/10.1093/mnras/stag594

UVIT Magellanic BRidge Analysis (UMBRA) – I. Far-UV–*Gaia* study of seven star clusters

Samyaday Choudhury [1,2★] Prasanta K. Nayak [3★] S. R. Dhanush,[4,5] Snehalata Sahu [6] and Richard de Grijs[7,8,9]

[1]*School of Arts and Sciences, Ahmedabad University, Ahmedabad, 380009, India*
[2]*International Centre for Space and Cosmology, Ahmedabad University, Ahmedabad, 380009, India*
[3]*Institute of Astrophysics, Pontificia Universidad Católica de Chile, Av. Vicuña Mackenna 4860, 7820436 Macul, Santiago, Chile*
[4]*Indian Institute of Astrophysics, 2nd Block Koramangala, Bangalore 560034, India*
[5]*Pondicherry University, R.V. Naga, Kalapet, Puducherry 605014, India*
[6]*Department of Physics, University of Warwick, Coventry CV4 7AL, UK*
[7]*School of Mathematical and Physical Sciences, Macquarie University, Balaclava Road, Sydney NSW 2109, Australia*
[8]*Astrophysics and Space Technologies Research Centre, Macquarie University, Balaclava Road, Sydney NSW 2109, Australia*
[9]*International Space Science Institute–Beijing, 1 Nanertiao, Zhongguancun, Hai Dian District, Beijing 100190, China*

Accepted 2026 March 19. Received 2026 March 17; in original form 2025 December 25

ABSTRACT

We present the first high spatial resolution far-ultraviolet (FUV; F148W) images of seven star clusters in the Magellanic Bridge using the UltraViolet Imaging Telescope (UVIT) on the Indian multiwavelength space observatory *AstroSat*. These observations emphasize UVIT's unique capability to resolve individual stellar populations at the distance of the Magellanic Clouds (50–60 kpc). Using probable cluster members, we constructed colour–magnitude diagrams using UVIT and *Gaia* data to estimate key cluster parameters such as age, distance, and extinction. We assessed the likelihood that these are genuine star clusters and carried out stellar parameter estimation of individual hot main-sequence (MS) stars. Our analysis confirms that four objects, BS 245, L 144, OGLE-MBR-CL-0075, and OGLE-MBR-CL-0084, are bona fide clusters. The remaining objects are likely OB associations or field stars. For three, OGLE-MBR-CL-0026, OGLE-MBR-CL-0030, and OGLE-MBR-CL-0084, we provide age estimates for the first time. All seven objects have ages between 15 and 70 Myr, supporting an *in situ* star formation scenario triggered by tidal interactions between the Magellanic Clouds. We further model the spectral energy distribution of 51 MS stars by combining photometric data from UVIT, the GALaxy Evolution eXplorer (*GALEX*), *Gaia*, and two near-infrared surveys: the VISTA Survey of the Magellanic Clouds and Two Micron All Sky Survey. The modelling reveals five hot MS stars with $T_{\rm eff}$ ranging between 32 500 (±1250) K to 42 500 (±1250) K and log *g* from 3.5 (±0.1) dex to 4.0 (±0.1) dex, consistent with late O-type stars. We release an FUV photometric catalogue of all MS stars to enable future studies of stellar abundances and binarity in the Bridge.

Key words: (stars:) Hertzsprung–Russell and colour–magnitude diagrams – (galaxies:) Magellanic Clouds – galaxies: star clusters: general – ultraviolet: stars.

1 INTRODUCTION

The Magellanic Bridge ('Bridge') is one of the characteristic signatures of the interaction between the Magellanic Clouds (MCs). It resembles a filamentary structure with lumps, holes, and shells, with an overall extent of 15–21 kpc. It has a total gas mass of $\approx 1.5 \times 10^8$ $M_\odot$ and an H I column density between 10^{20} and 10^{21} cm^{-2} (L. Staveley-Smith et al. 1998; E. Muller et al. 2003). The Bridge is said to have formed during the most recent encounter (≈100–300 Myr ago) between the MCs (see G. Besla et al. 2012, and references therein). Studies have proven that the Bridge contains a blue and young stellar population (M. J. Irwin, W. E. Kunkel & S. Demers 1985; J. Harris 2007; C. H. R. Chen et al. 2014; D. M. Skowron et al. 2014) that is bright at ultraviolet (UV) wavelengths. This population is present in the form of stellar aggregates, such as star clusters, which can be used to estimate ages, metallicities, distances and extinction in, to and across the Bridge. These parameters are crucial for estimating the star formation history, morphology, and chemical enrichment in the Bridge.

Periodic interactions between the Clouds have led to episodes of star cluster formation, with the most recent interaction manifested by the presence of young, <500 Myr-old cluster candidates (e.g. G. Pietrzynski & A. Udalski 2000; P. K. Nayak et al.

★ E-mail: samyaday.choudhury@ahduni.edu.in (SC); nayakphy@gmail.com (PKN)

2016, 2018; S. R. Dhanush et al. 2024). To date, the largest catalogue of star cluster candidates (∼3700 entries) in the MCs and Bridge region has been prepared by E. Bica et al. (2008, hereafter B08).

Photometric surveys that aimed to cover the outer areas of the MCs, for example, the Optical Gravitational Lensing Experiment IV (OGLE IV; A. Udalski, M. K. Szymański & G. Szymański 2015), the Survey of the Magellanic Stellar History (SMASH; D. L. Nidever et al. 2017), and the VISTA Survey of the Magellanic Clouds (VMC; M. R. L. Cioni et al. 2011), have led to the discovery of new cluster candidates in the outskirts of the MCs, including in the Bridge region (e.g. A. E. Piatti et al. 2015; M. Sitek et al. 2016, 2017). M. Sitek et al. (2016, 2017) catalogued about 300 newly discovered cluster candidates in the outskirts of the MCs and in the Bridge based on the OGLE IV survey. Recently, E. Bica et al. (2020, hereafter B20) compiled the most updated catalogue of known star clusters in the Small Magellanic Cloud (SMC) and the Bridge. B20 emphasized the importance of scrutinizing the new OGLE IV and SMASH clusters in the SMC's halo and Bridge to disentangle the young clusters from tidally stripped halo or disc clusters in the MCs. Only 75 per cent of B20's catalogue entries have associated age information from past studies. However, only 626 of the total number of 2741 entries are confirmed clusters, i.e. just 23 per cent. This shows that although previous studies (e.g. E. Bica et al. 2015, hereafter B15; also R. A. P. Oliveira et al. 2023) have aimed to estimate the physical properties (ages, metallicities, distances) of previously and newly identified clusters in the Bridge, the number of well-parametrized Bridge clusters is far from complete.

This paper is an initiative to estimate the parameters of such star clusters in the Bridge, while also verifying their physical reality and identifying any possible discrepancies with respect to their categorization and parameter estimates in past studies of young star clusters. Young star clusters are best traced and studied at UV wavelengths, compared with optical and near-infrared (NIR) wavelengths. UV-bright populations were easily detected in GALaxy Evolution eXplorer (*GALEX*) UV images (D. C. Martin et al. 2005) of the Bridge. However, the *GALEX* mission was limited by its angular resolution of ∼5 arcsec, which is insufficient to study individual stars at the distances of the MCs, approximately 50 and 62 kpc for the Large Magellanic Cloud (LMC) and the SMC, respectively (R. de Grijs, J. E. Wicker & G. Bono 2014; R. de Grijs & G. Bono 2015). The Ultraviolet Imaging Telescope (UVIT) onboard *AstroSat* has three times better spatial resolution (∼1.4 arcsec) compared with *GALEX* (S. N. Tandon et al. 2020) and has proven suitable for probing UV-bright star clusters in the MCs (P. K. Nayak et al. 2021) as well as young stellar populations in the SMC (S. Hota et al. 2024a, b). We conducted a UVIT programme to observe four regions in the Bridge located towards the East of the SMC. Young and UV-bright stars present a higher concentration closer to the SMC Wing and another halfway between the MCs, with a strong correlation to the distribution and kinematics of the H I gas (e.g. D. M. Skowron et al. 2014; C. E. Murray et al. 2019; P. Zivick et al. 2019). These identified UV-bright star clusters were either not parametrized or do not have well-constrained ages owing to a lack of high-resolution UV data.

In this first paper of a series, we present the results of seven young star clusters observed within the four UVIT tiles. These clusters were identified from the B08 and M. Sitek et al. (2017) catalogues. Four clusters (BS 245, L 144, OGLE-MBR-CL-0070, and OGLE-MBR-CL-0075) have previous age estimates based on optical [e.g. E. Bica et al. (2015, hereafter B15); R. A. P. Oliveira et al. (2023)] and NIR data (e.g. A. E. Piatti et al. 2007), whereas three clusters (OGLE-MBR-CL-0026, OGLE-MBR-CL-0030, and OGLE-MBR-CL-0084) have no previous age estimates reported in literature. The selection of clusters discussed in this paper was based on the criteria that some had previous estimates of ages for validation of our technique through comparison, and a few had not been studied at all. Forthcoming papers in this series will cover all other UV-bright stellar aggregates in the UVIT-observed fields in the Bridge. A comparison of UV image cut-outs between *GALEX* and UVIT for all clusters is presented in Figs 1 and 2 to highlight the superior quality of the UVIT images.

The Bridge represents a unique environment (metal-poor, low gas density, and tidally stripped) that supports the formation of massive, OB-type stars (e.g. V. Ramachandran, L. M. Oskinova & W. R. Hamann 2021). Many studies have thus far focused on deciphering the stellar properties of OB stars in the discs of the LMC and the SMC (e.g. D. Crampton & J. Greasley 1982; P. Massey et al. 1995; J. B. Lamb et al. 2016) but not in the Bridge. Only recently, V. Ramachandran et al. (2021) discovered the first three O-type stars in the Bridge. In the past, D. I. Casetti-Dinescu et al. (2012) mapped the possible spatial distribution of OB stars as observed by *GALEX* and showed a dense distribution of such stars in the Bridge, closer to the south-eastern section of the SMC. These stars are located in stellar aggregates, such as young star clusters and OB associations. Estimation of their spectral properties is key to unlocking the underlying processes behind recent star formation, stellar feedback into the interstellar medium (ISM) and rotation properties of OB stars in the Bridge (V. Ramachandran et al. 2021). However, in the absence of spectra, constructing spectral energy distributions (SEDs) of stars using multiwavelength data (far-UV/FUV to NIR) helps estimate key stellar properties ($T_{\rm eff}$ and $\log g$) and points to interesting targets for future high-resolution spectroscopic studies. UVIT's resolution in FUV images could help identify such stars within star clusters in the Bridge. To facilitate the identification of such stars, we release a photometric catalogue of FUV sources associated with our seven target objects, identified using UVIT, which could be cross-matched with the publicly available datasets used in this work.

This paper is organized as follows. Section 2 contains the details of the observations and data used. Section 3 contains the parametrization of star clusters and a discussion of individual clusters. The estimation of stellar parameters for hot, OB-type main-sequence (MS) stars in each cluster is presented in Section 5. Section 6 contains a discussion of the results, whereas the summary is presented in Section 7.

2 DATA

UVIT comprizes two telescopes with apertures of 38 cm, with a field of view of 28 arcmin and a spatial resolution of ∼1.4 arcsec. UVIT observes in three channels: FUV (130–180 nm), near-UV (NUV; 200–300 nm) and visible (VIS; 350–550 nm), where each channel has multiple distinct filters, ranging from wide to narrow bands (S. N. Tandon et al. 2020). We observed four tiles (Proposal ID: A09_012, July–August 2020, PI: Choudhury) in the *F*148*W* channel (the widest UVIT FUV filter; $\lambda_{\rm eff} \approx 148$ nm, range $\approx$ 125–180 nm). Their details are provided in Table 1. Unfortunately, the NUV channel was inactive because of technical problems during the observation period. We downloaded the Level 1 data

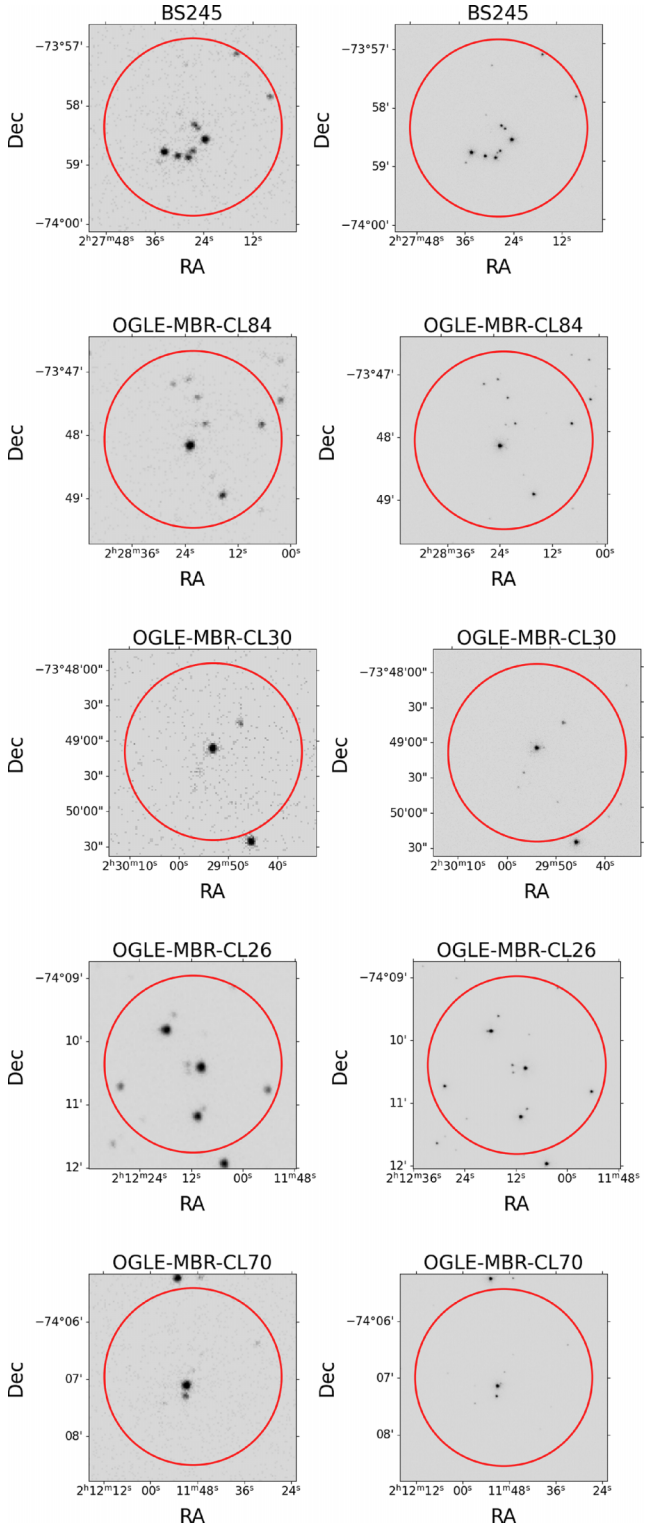

Figure 1. *GALEX* versus UVIT image for clusters in Tile 1: BS 245, OGLE-MBR-CL-0084 and OGLE-MBR-CL-0030; and Tile 2: OGLE-MBR-CL-0026 and OGLE-MBR-CL-0070. The panels illustrate the superior resolution of UVIT (right) compared with *GALEX* images (left). The open circle shows three times the cluster radii mentioned by B08 and M. Sitek et al. (2017), which we considered as the cluster region for our analysis.

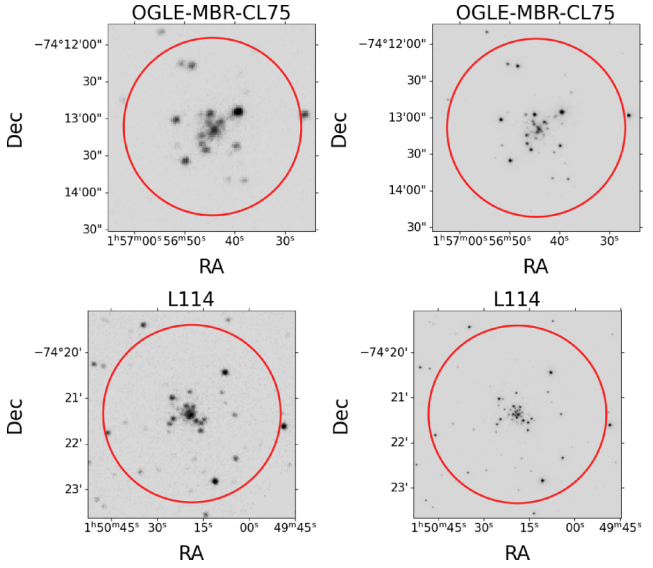

Figure 2. *GALEX* versus UVIT image for clusters OGLE-MBR-CL-0075 (Tile 3) and L 114 (Tile 4). Technical details are as for Fig. 1.

Table 1. Coordinates of UVIT observed tiles and corresponding exposure times in the FUV *F*148*W* filter. The size of each tile is 28 arcmin.

UVIT Tile	(RA °, Dec.°)	Exposure time (s)
Tile-1	37.16, −73.87	2382
Tile-2	33.26, −74.08	2412
Tile-3	29.50, −74.24	2380
Tile-4	27.87, −74.24	1971

from the *AstroSat* portal[1] and processed them using the customized software CCDLAB to produce science-ready images (J. E. Postma & D. Leahy 2017). Processing includes running tasks such as drift correction, flat-fielding, alignment, correction for intrinsic distortion and correction for fixed detector pattern noise (J. Postma, J. B. Hutchings & D. Leahy 2011; V. Girish et al. 2017).

We carried out point spread function (PSF) photometry of all observed tiles using the DAOPHOT package of the Image Reduction And Analysis Facility tool (IRAF; P. B. Stetson 1987), following standard techniques. The technique followed is similar to that described by S. Hota et al. (2024a, their section 2.2). Note that the PSF model was generated by selecting seven to eight stars of different fluxes (varying brightnesses) in each tile, from uncrowded fields. This reduces any bias towards a given magnitude. Fig. 3 (top) shows the error in magnitude ($e_{\rm F148W}$) versus magnitude for Tile 1; $e_{\rm F148W}$ is $\lesssim$0.1 mag (i.e. S/N $\geq$ 100) for all magnitudes >21 mag. Note that UVIT magnitudes are given in the AB system; we converted the UVIT *F*148*W* magnitudes to the Vega system for our analysis. All stars used for parameter estimations typically have sharpness between ±0.75, which confirms that we considered only point sources. Fig. 3 (bottom) shows that the *F*148*W* magnitudes are > 90 per cent complete for values <21 mag, and ≈ 100 per cent complete for *F*148*W*<

[1] https://astrobrowse.issdc.gov.in/astro_archive/archive/Home.jsp

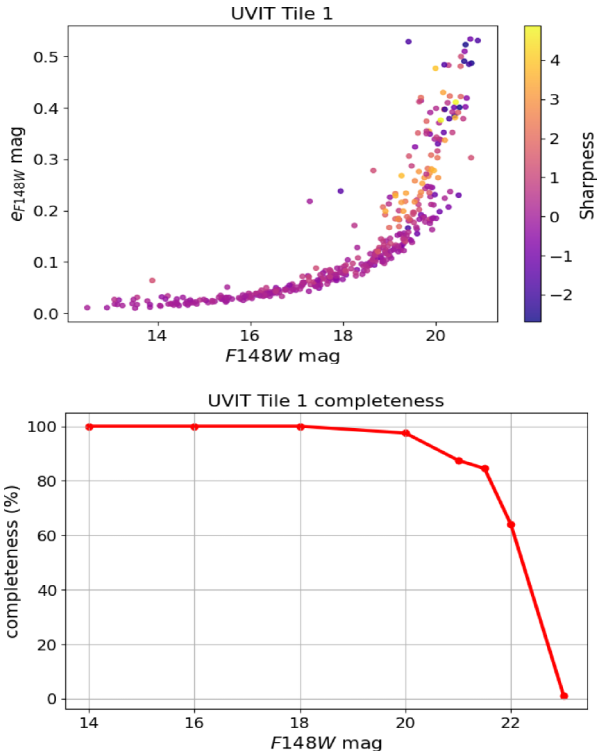

Figure 3. Top: Error in magnitude versus $F148W$ PSF magnitude (Vega system) for Tile 1.
The colour bar denotes sharpness values. Bottom: Completeness derived for Tile 1 using artificial star tests.

19 mag. The outer edges of each tile had issues related to object detection, hence the need for PSF estimates. None of the studied clusters is located near the outer edges; they are all located <12 arcmin from the tile centres (the radius of each UVIT tile is $\approx$ 14 arcmin).

One of the aims of this study is to characterize the SED of the UV-bright MS stars in the clusters. In addition to the FUV, the NUV is also sensitive to $T_{\rm eff}$ variations in these hot MS stars and can thus help improve the accuracy of the best-fitting SED parameters. However, UVIT observations in NUV filters were unavailable for this project. To address this, we used the archival UV intensity maps (exposure times ranging from 914 to 1646 s) from *GALEX* DR6 (L. Bianchi, A. Conti & B. Shiao 2014) as part of the Nearby Galaxies Survey (NGS). We performed PSF photometry following the same procedure as for UVIT to obtain the *GALEX* NUV magnitudes. Note that the *GALEX* resolution (4–5 arcsec) is comparatively poorer than UVIT's, especially in the NUV, which suffers from crowding in the central regions of dense and compact clusters. However, NUV magnitudes are reliable for sources located on the outskirts of a cluster or in less dense clusters that are well-resolved. For optical data, we used the *Gaia* DR3 photometric (G, BP, RP) and astrometric (proper motion/pm, parallax) catalogue (Gaia Collaboration 2023). For the NIR, we used the Y, J, and $K_{\rm s}$ passbands from VMC DR6, which we obtained from the PSF photometry catalogue available from the ESO Science Archive Facility (https://www.eso.org/qi/catalog/show/401), and Two Micron All Sky Survey (2MASS) J, H, $K_{\rm s}$ data where VMC was unavailable.

3 ANALYSIS OF UV-BRIGHT STAR CLUSTERS IN THE BRIDGE

3.1 Cluster sample

We selected our star clusters from the catalogues of B08 and the newly identified clusters in the OGLE IV survey (M. Sitek et al. 2017). These clusters are spatially sparse (a few 100–1000 stars, as defined by P. K. Nayak et al. 2016, 2018) compared with the rich clusters usually found in the MCs (A. D. Mackey 2009, and references therein) and located in four of the observed UVIT tiles. Initially, we defined the cluster radii as the mean of semimajor and semiminor axes in B08 and extracted five times the cluster radii from the *Gaia* DR3 catalogue for our analysis. We attempted to estimate the cluster radii using the radial density profile, but most clusters lacked a spatial density profile in the G and $F148W$ bands).

Assuming the cluster to be confined within the radius determined by B08 and M. Sitek et al. (2017), we were left with only a few MS stars in the cluster colour–magnitude diagrams (CMDs), making them unsuitable for estimating parameters. We inspected the FUV images for all cases, which showed a small number of FUV-bright stars located away from the cluster centre (see Figs 1 and 2). These stars may have been produced in young clusters or in OB associations. Hence, we decided to carry forward our analysis by considering stars within a larger area than the cluster radii listed in previous catalogues. In most cases, selecting thrice the cluster radius helped include this fraction of FUV-bright stars and produced a MS that could be fitted adequately with isochrones. Selecting a larger radius than included in the catalogue may increase the possibility of adding contamination from the Galaxy and the Bridge's field region. Therefore, we used cut-offs in parallax and pm (see Sections 3.2 and 3.3) to identify potential cluster members.

3.2 Removal of Galactic contamination

We removed the Milky Way foreground contamination from the cluster region using *Gaia* parallax and pm values. We selected stars with parallaxes between $\pm$1 mas ($\sim 1\sigma$ around the mean), and pm (in RA and Dec.) within $\pm$3 times the standard deviation about their mean values. Fig. 4 shows an example result of removing Galactic counterparts for one of the clusters, L 114. Three panels show a comparison of the distributions of parallax, pmra and pmdec (top left, top right and bottom left, respectively) for all stars within the cluster region for our assumed cuts. The bottom right-hand figure shows that, after adopting these cuts, most stars are located in the clumpy region of the two-dimensional pm plane, with the outliers excluded. The stars' spatial plot (see Section 3.3) after applying the cuts also reveals a clumpy distribution in the RA versus Dec. plane compared with the surrounding region. This indicates that these stars could be probable cluster candidates. Similar figures for the remaining clusters are presented in Appendix B.

3.3 Cluster membership based on the KDE method

We attempted to clean the cluster CMDs using the field-star decontamination techniques described by S. Choudhury, A. Subramaniam & A. E. Piatti (2015), which involve defining a box of growing size in colour and magnitude around a star in the

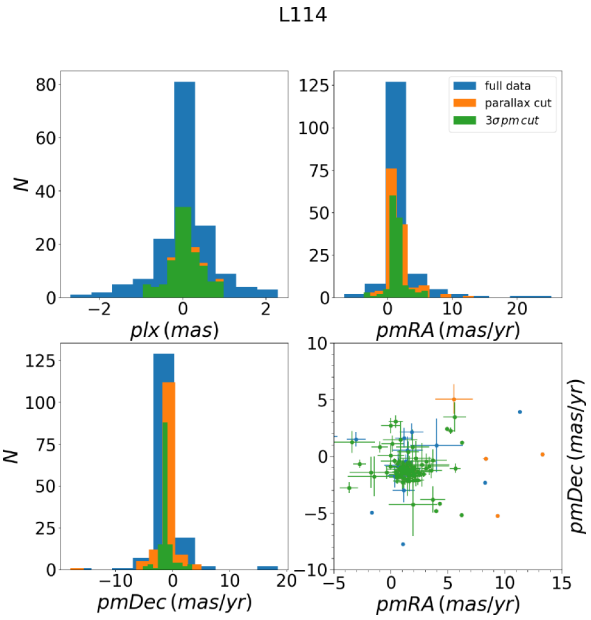

Figure 4. Distribution of stars after parallax and pm cuts in RA and Dec., shown in the top right, top left and bottom left-hand panels, respectively. 'Full data' contains all *Gaia* data within the assumed cluster radius. The bottom right-hand panel shows the clumping in the pmDec versus pmRA plane, including the errors. With the assigned cuts, stars in the clumpy region are retained, as indicated by the green points.

cluster's CMD and checking for any counterpart in an annular field CMD. If a field-star counterpart is found, the cluster star is not considered a member. The same technique was employed by P. K. Nayak et al. (2016, 2018). However, $(G, BP - RP)$ CMDs for the cluster and field contain only a small number of stars, and this cleaning technique did not yield satisfactory results. Beyond distances of 1 kpc (parallax = 1 mas) the errors in parallax are of similar order of magnitude as the parallax values, implying that parallax values are less reliable for distances of the MCs. Hence, we decided to place constraints on the pm values. We employed a kernel density estimation (KDE) technique to identify stars with the highest probable membership using the two-dimensional pm plane (pmDec versus pmRA). We estimate the density distribution in the two-dimensional pm plane by binning it into a grid of 50 bins along the pmRA and pmDec axes. We smoothed the density diagram using Gaussian kernels; see Fig. 5 (top). Next, we selected the stars from within the 50th and 84th percentiles of the KDE. Their distribution in the pm plane is shown in Fig. 5 (middle). It shows that stars within the 50th percentile cover most of the clumpy part of the distribution, whereas those within the 84th percentile are few in number, are located only centrally concentrated and result in only a few stars remaining for CMD analysis. Thus, we adopt a 50th percentile cut in the pm plane as our probable cluster members.

Fig. 5 (bottom) shows a spatial plot of L 114. The cluster is observed as a density-enhanced clump in the centre. We overplotted the UVIT cross-matched data with *Gaia* (search radii of 1 arcsec). Next, we overplotted the probable cluster members (50th percentile of the pm KDE). Most FUV-bright (MS) stars selected after applying all of the above cuts are found to be centrally concentrated, in agreement with the mass-segregation scenario of hot (massive) stars in star clusters. This plot further validates our cut-off criteria in parallax, a 3σ deviation from the mean pm and

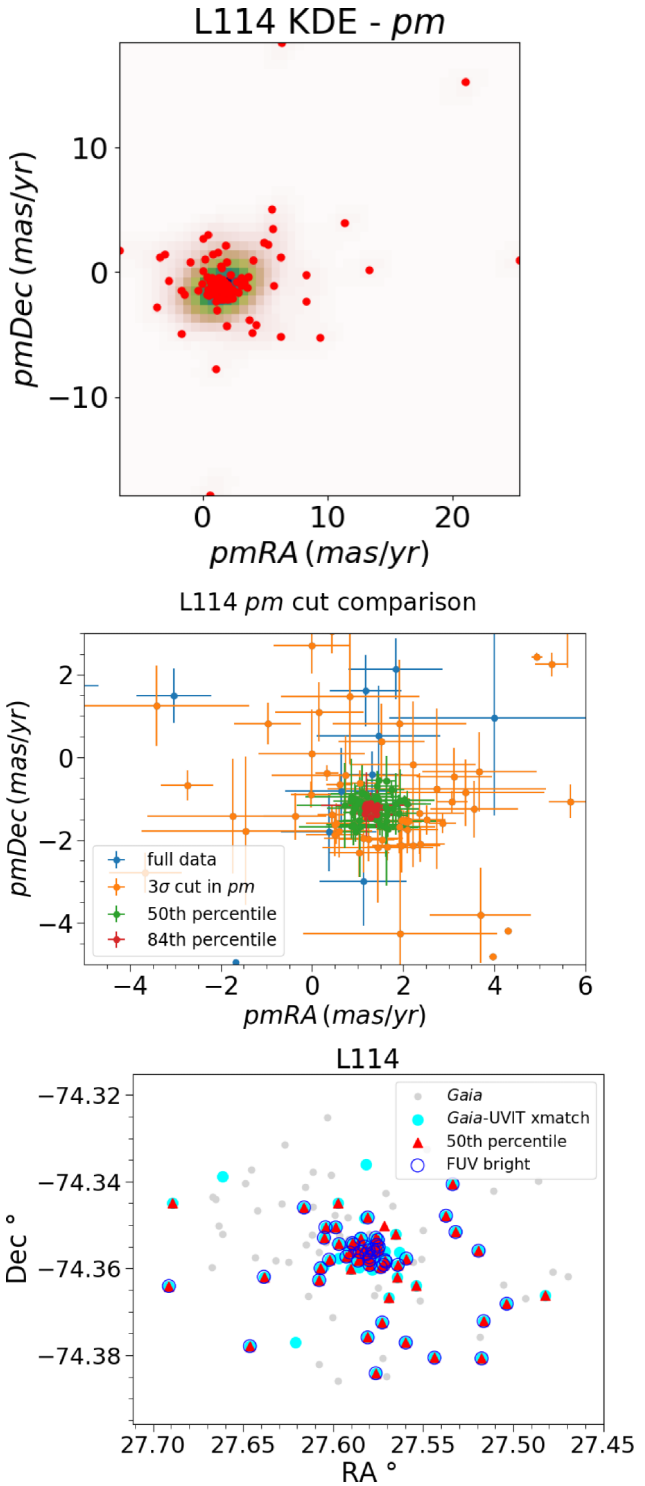

Figure 5. For cluster L 114: The top panel shows the KDE estimation in the 2D pm plane, with all stars overplotted as red points. The middle panel shows the 50th and 84th percentile stars overplotted on the KDE. The bottom panel shows the spatial plot of *Gaia* (grey circles), *Gaia*–UVIT cross-matched stars (cyan circles), 50th percentile stars (red triangles) and only the FUV-bright stars (blue open circles).

a cut at the 50th percentile in the KDE–pm plane, which is representative of cluster members. The cluster members are bright in the UV; hence, UV CMDs are the best way to estimate their parameters (ages, extinction and distance moduli/μ_0). However,

Table 2. Estimated parameters of the seven cluster candidates.

UVIT Tile no.	Cluster name	RA° *(J2000)*	Dec.° *(J2000)*	A_G (mag)	μ_{0G} (mag)	Age ($\log \tau_G$) (dex)	$A_{\rm F148W}$ (mag)	$\mu_{0\rm F148W}$ (mag)	Age ($\log \tau_{\rm F148W}$) (dex)
1	BS 245	36.86	−73.97	0.27	18.50	7.10	1.30	18.75	7.20
1	OGLE-MBR-CL-0084	37.09	−73.8	0.10	18.00	7.7	0.50	18.50	7.55
1	OGLE-MBR-CL-0030	37.47	−73.82	0.33	18.00	7.45	0.40	18.50	7.45
2	OGLE-MBR-CL-0026	33.05	−74.17	0.10	18.50	7.35	1.10	18.50	7.25
2	OGLE-MBR-CL-0070	32.96	−74.12	0.17	18.75	7.45	1.10	18.25	7.20
3	OGLE-MBR-CL-0075	29.19	−74.21	0.17	18.50	7.80	0.80	18.25	7.85
4	L 114	27.58	−74.36	0.27	18.0	7.80	1.10	18.25	7.80

Note. Parameters estimated using (G, $BP-RP$) CMDs are listed in columns 5–7, whereas those estimated using *(F148W, F148W-G)* CMDs are listed from columns 8–10.

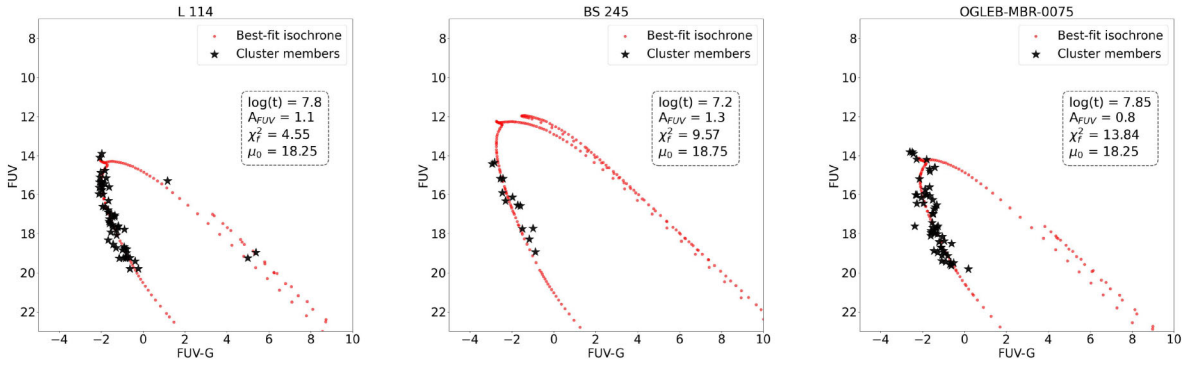

Figure 6. ($F148W$, $F148W-G$) CMDs of star clusters with prominent cluster features: L 114 (56), BS 245 (13) and OGLE-MBR-CL-0075 (56). The numbers in parentheses indicate the final numbers of stars fitted in each CMD.

in the absence of UVIT NUV data, we used ($F148W$, $F148W-G$) CMDs for parameter estimation. To verify our estimates, we also used (G, $BP-RP$) CMDs. Note that figures similar to Fig. 5 are presented in Appendix B for individual clusters.

3.4 Estimation of ages, extinction, and distances

The ages, extinction values, and distance modulus (μ_0) of the clusters were determined using the approach described by S. R. Dhanush et al. (2024, hereafter D24). The theoretical isochrones for the UVIT and *Gaia* filters were obtained from the PARSEC stellar evolutionary models (A. Bressan et al. 2012). We used a constant metal fraction, $Z = 0.004$, which represents the SMC, to estimate the cluster parameters. Our sample clusters are expected to have ages <200 Myr, the time-scale of the most recent interaction between the Clouds. Hence, we used a constant metal fraction to avoid parameter degeneracy during the isochrone fitting process. We used an age range of $\log(t\ \mathrm{yr}^{-1}) = 6$–$8.2$ (1 Myr to ∼ 160 Myr), with a spacing of $\Delta \log(t\ \mathrm{yr}^{-1}) = 0.05$ to perform the fitting. Moreover, we select a μ_0 range of 17–19 mag (e.g. B15, R. A. P. Oliveira et al. 2023) with a step size of 0.25 mag; an extinction range from 0 to 0.832 (ΔA_G) with a step size of 0.025 mag in the G band, and 0 to 2.65 mag ($\Delta A_{\rm F148W}$) with a step size of 0.1 mag in the FUV band to fit the ($F148W$, $F148W-G$) and (G, $BP-RP$) CMDs, respectively. The modified χ^2 values ($\chi^2_{\rm f}$), as defined by D24, were estimated for each of the cluster samples.

We compared the resulting $\chi^2_{\rm f}$ values for individual clusters and selected the model with the lowest $\chi^2_{\rm f}$ as the best fit. The corresponding physical parameters for each star cluster are summarized in Table 2. The parameter step sizes in the fitting process were carefully chosen to ensure that the true minimum was found and that it falls within the 68.3 per cent confidence region. For fits involving three parameters, the 68.3 per cent confidence interval is defined as the region where the parameter values satisfy $\chi^2 < \chi^2_{\rm min} + 3.53$, following the standard deviation of the χ^2 distribution for three degrees of freedom. This approach yields uncertainties of approximately ± 0.10 dex in age, ± 0.20 mag in μ_0, ± 0.02 mag in A_G and ± 0.06 mag in $A_{\rm F148W}$. Note that the clusters examined in this study are young, with stars predominantly in the MS phase, which constrains the precision of parameter estimates. The χ^2 method was preferred with respect to Bayesian inference techniques to avoid inefficient exploration of parameter space in cases where the small number of stars (a few tens) in the MS limits model fitting. Nevertheless, our parameter estimates are robust and provide a reliable basis for further investigation.

4 INDIVIDUAL CLUSTERS

In this section, we present the results for the individual clusters and compare them with those of previous studies, tile-wise. Based on their CMDs and their spatial plots, we draw inferences as to any discrepancy compared with their previous categorization by B08 and M. Sitek et al. (2017) as star clusters. Note that for three of the seven objects, we have estimated properties (age, extinction and μ_0) for the first time. The ($F148W$, $F148W-G$) and (G, $BP-RP$) CMDs for the clusters with prominent features (L 114, BS 245, and OGLE-MBR-CL-0075) are presented in Figs 6 and 8, respectively. The ($F148W$, $F148W-G$) and (G, $BP-RP$) CMDs for the clusters with sparsely populated features (OGLE-MBR-CL-0026, OGLE-MBR-CL-0030, OGLE-MBR-CL-0070, and OGLE-MBR-CL-0084) are presented in Figs 7 and 9, respectively.

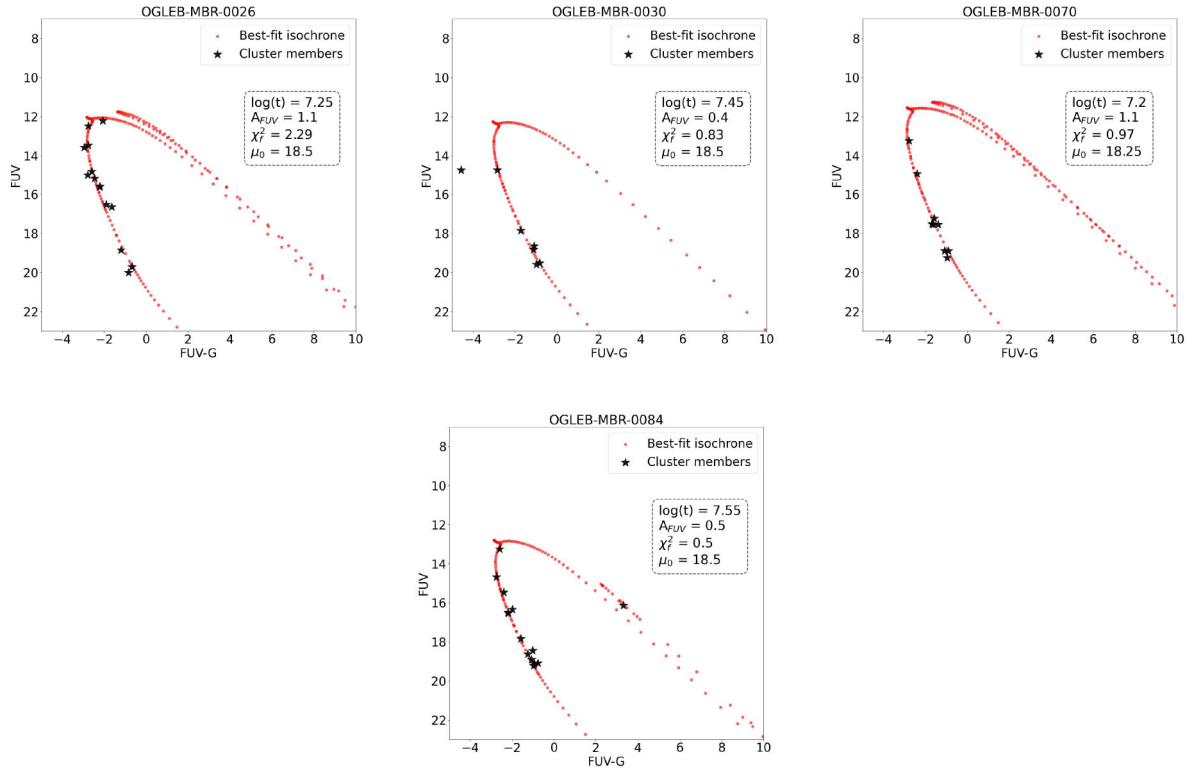

Figure 7. As Fig. 6, but for star cluster candidates with sparsely populated MSs: OGLE-MBR-CL-0026 (14), OGLE-MBR-CL-0030 (7), OGLE-MBR-CL-0070 (9), and OGLE-MBR-CL-0084 (14).

4.1 BS 245

BS 245 (Tile 1): BS 245 was classified as CA (cluster similar to association) by B08. We estimated very similar ages of 12 Myr (log $\tau_G = 7.1 \pm 0.1$) and 16 Myr (log $\tau_{\rm F148W} = 7.2 \pm 0.1$) from the ($G$, $BP - RP$) and ($F148W$, $F148W{-}G$) CMDs, respectively (see Figs 6 and 8). The ages are younger than those estimated by B15; $\approx$ 100 Myr (log $\tau = 8.00 \pm 0.25$). B15 used deep BVR data from the 4 m SOAR telescope and detected a few MS stars in the cluster's (V, $B - V$) CMD. Their fig. 5 shows the presence of some blue stars around the cluster centre in the composite BVR image, which appear saturated. UVIT's $F148W$ image distinctly resolves such stars, and they are found to be FUV-bright (see Fig. 1). Note that B15 did not apply parallax and pm cuts. Moreover, owing to small-number statistics, B15 did not use a numerical-statistical isochrone fitting method to estimate the age, μ_0 and extinction of BS 245. Rather, they used a visual isochrone fit to estimate its parameters. In comparison, we carried out cluster membership analysis using parallax, pm, and KDE cuts to provide further assurance as regards the membership probabilities and used a χ^2 fitting algorithm for parameter estimation.

Our estimated μ_0s are 18.5 ± 0.20 and 18.75 ± 0.20 mag, based on the (G, $BP - RP$) and (F148W, F148W$-G$) CMDs, respectively. These values agree within $\pm 1\sigma$, suggesting that the cluster is located closer to the LMC's distance. B15 estimated the distance to be relatively closer compared with our results ($\mu_0 = 18.0 \pm 0.30$ mag). We used $Z = 0.004$, whereas, B15 estimated $Z = 0.008 \pm 0.006$. Their Z is similar to that of the LMC but agrees well with our assumption, owing to the high uncertainty in their Z estimates. Assuming a constant μ_0 but two different Z values (0.004 and 0.008) would not help in accounting for the difference in ages observed between our and B15's results. However, if we assume $Z = 0.004$ for an isochrone of 20 Myr, and if the μ_0 is decreased by 0.5 mag, the MS could be fitted by a 100 Myr-old isochrone. This could have caused B15 to estimate relatively older ages for BS 245 compared with ours. B15 estimated almost zero reddening ($E(B - V) = 0.01$ mag) and, hence, negligible extinction ($A_V = 0.03$ mag) towards BS 245. We estimated $A_V = 0.32 \pm 0.02$ mag and 0.49 ± 0.02 mag from the (G, $BP - RP$) and ($F148W$, $F148W{-}G$) CMDs, respectively. Our method incorporates quality cuts to define cluster membership, and the parameter estimation is statistically more rigorous compared with B15, and is thus free from visual biases.

4.2 OGLE-MBR-CL-0030

OGLE-MBR-CL-0030 (Tile 1): This was a newly identified cluster candidate by M. Sitek et al. (2017) based on OGLE-IV survey data. We did not observe any spatial clumping of stars in the FUV images or in *Gaia* spatial plots. The (G, $BP - RP$) and ($F148W$, $F148W{-}G$) CMDs are sparsely populated with only a few faint stars and a single optically or FUV- bright star separated by 2–3 mag (see Figs 7 and 9). A distinct MS feature is lacking. Based on the spatial plots and sparsely populated CMDs, it is difficult to categorize this object as a genuine cluster. It could instead be an OB association or field MS stars. The estimated ages derived from the (G, $BP - RP$) and ($F148W$, $F148W{-}G$) CMDs are similar, $\approx$28 Myr (log $\tau = 7.45 \pm 0.1$). The estimated μ_0 are 18.0 ± 0.20 mag and 18.50 ± 0.20 mag based on the (G, $BP - RP$) and ($F148W$, $F148W{-}G$) CMDs, respectively. These values agree within $\pm 2\sigma$. The estimated extinction values are $A_V = 0.39 \pm 0.02$ mag and 0.15 ± 0.02 mag based on the (G, $BP - RP$) and ($F148W$, $F148W{-}G$) CMDs, respectively. They are significantly

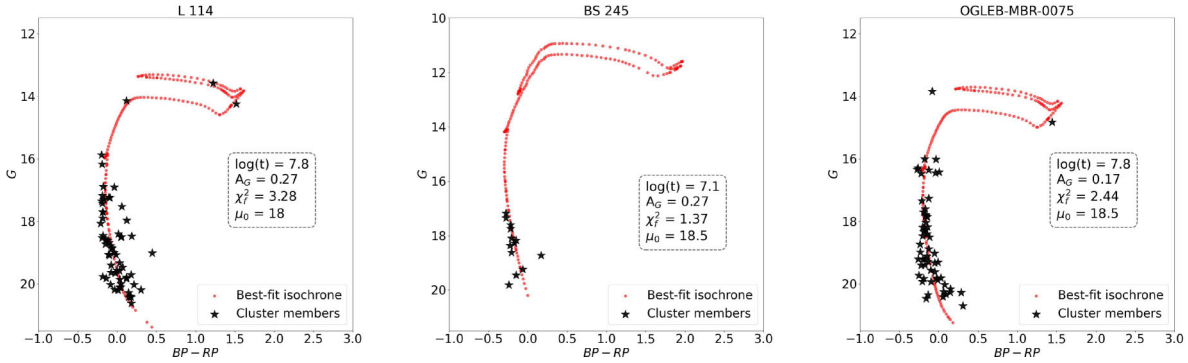

Figure 8. (G, $BP - RP$) CMDs of star clusters with prominent cluster features: L 114 (63), BS 245 (13), and OGLE-MBR-CL-0075 (58). The numbers in parentheses indicate the final numbers of stars fitted in each CMD.

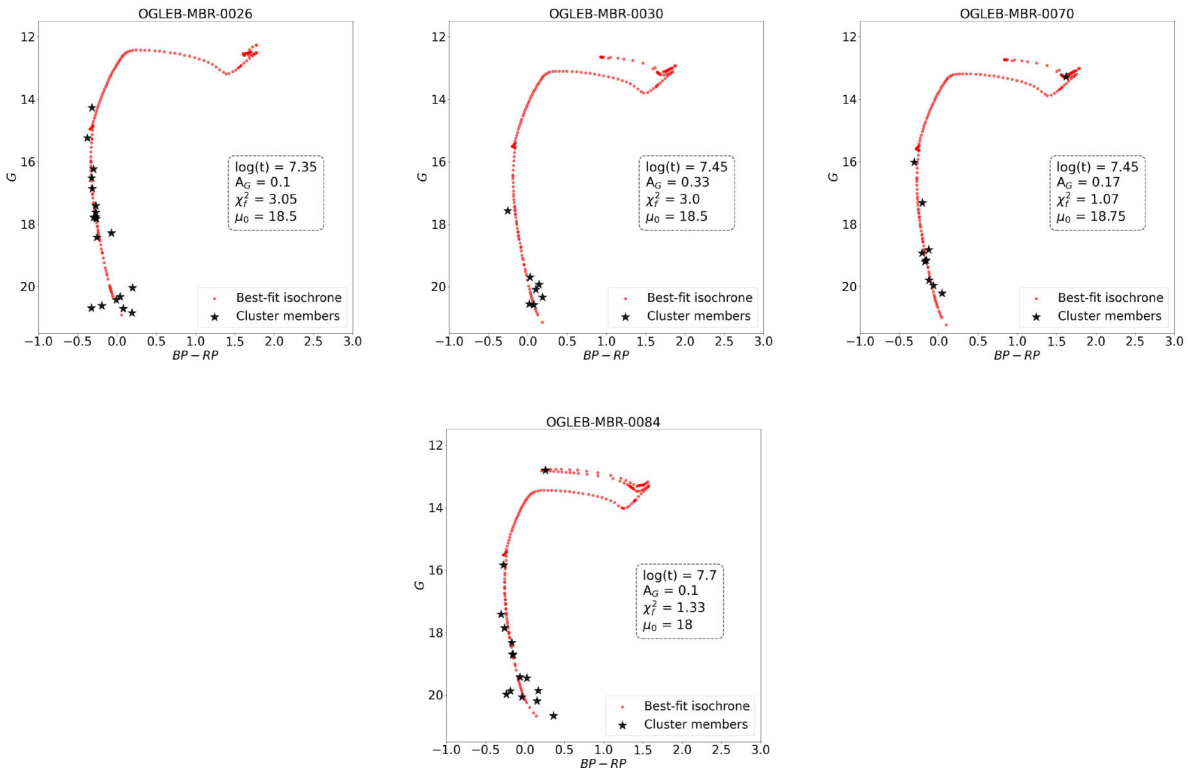

Figure 9. As Fig. 8, but for star cluster candidates with sparsely populated MSs: OGLE-MBR-CL-0026 (19), OGLE-MBR-CL-0030 (7), OGLE-MBR-CL-0070 (10), and OGLE-MBR-CL-0084 (15).

different from each other. Note that the uncertainty in the A_G and $A_{\rm F148W}$ estimates translates to similar values in A_V, i.e. ± 0.02 and ± 0.02 mag, respectively, considering the propagation of errors. Although we present the parameters of OGLE-MBR-CL-0030 for the first time, note that the object's parametrization is affected by the absence of a well-defined MS similar to an isochrone. The (dis)similarities in the estimated parameters are indicative of this. Hence, we avoid interpreting these values.

4.3 OGLE-MBR-CL-0084

OGLE-MBR-CL84 (Tile 1): This was listed as a cluster in the newly compiled catalogue of B20. We did not observe any spatial density enhancement in *Gaia* DR3 or in the spatial distribution of FUV-bright MS stars. Some FUV bright stars are found near the cluster centre (see Fig. 1). The (G, $BP - RP$) and ($F148W$, $F148W-G$) CMDs are sparsely populated (10–12 stars each), but they populate the MS almost equally at different magnitudes and follow the trend of the isochrone (see Figs 7 and 9).

If we assume that these stars represent stellar aggregates born from the same progenitor molecular cloud, their ages are $\sim$35 Myr ($\log \tau_{\rm F148W} = 7.55 \pm 0.10$) and 50 Myr ($\log \tau_G = 7.70 \pm 0.10$) based on the ($F148W$, $F148W-G$) and (G, $BP - RP$) CMDs, respectively; they are consistent within $\pm 1\sigma$. The estimated μ_0 values are 18.50 ± 0.20 and 18.0 ± 0.20 mag, respectively, reasonably consistent within $\pm 2\sigma$. This suggests that the object is located at a similar distance as the LMC, or closer. The estimated extinction values are $A_V = 0.19$ and 0.12 mag, respectively, consistent within $\pm 3\sigma$. We therefore support the categorization of B20 and present, for the first time, an estimate of the key physical parameters.

4.4 OGLE-MBR-CL-0026

OGLE-MBR-CL-0026 (Tile 2): This cluster was newly identified by M. Sitek et al. (2017) based on OGLE-IV. A small clump was observed in the *Gaia* spatial plot, and a few UV-bright stars were observed around the cluster centre. A sparsely populated but distinct cluster MS was identified in the (G, $BP-RP$) and ($F148W$, $F148W-G$) CMDs (see Figs 7 and 9). We estimated an age of ≈20 Myr and $\mu_0 = 18.50 \pm 0.20$ mag from both CMDs. Our results confirm the presence of a young stellar aggregate located at the LMC's distance. The estimated A_V values are 0.12 ± 0.02 and 0.41 ± 0.02 mag based on the (G, $BP-RP$) and ($F148W$, $F148W-G$) CMDs, respectively. The large discrepancy of $\pm 15\sigma$ between the two values may be owing to one of two reasons, including a small number of MS stars (≈10 with $F148W < 19$ mag) and a larger spread in ($F148-G$) colour (≈ 0.2 mag) compared with the equivalent ($BP-RP$) colour spread (< 0.05 mag); for more discussions, see Section 6. We have estimated the parameters of OGLE-MBR-CL-0026 for the first time in this study.

4.5 OGLE-MBR-CL-0070

OGLE-MBR-CL-0070 (Tile 2): Estimates using the ($F148W$, $F148W-G$) and (G, $BP-RP$) CMDs suggest ages of ∼16 Myr ($\log \tau_{F148W} = 7.20 \pm 0.10$) and 28 Myr ($\log \tau_G = 7.45 \pm 0.10$), respectively, which agree well within $\pm 1.5\sigma$ (see Figs 7 and 9). B15 had earlier detected a few MS stars in (V, $B-V$) CMDs and classified this object as a cluster. We did not observe any clumping in the spatial plot and verified that the CMD indeed contains a few MS stars. A. E. Piatti et al. (2015) categorized this object as a 'possible non-cluster' or 'not-recognized' by analysing NIR data from the VMC survey. A. E. Piatti et al. (2015)'s interpretation is in agreement with the observations that OGLE-MBR-CL-0070 contains young stars that are bright in the FUV and optical. The F148W images show two FUV-bright stars at the centre of OGLE-MBR-CL-0070. The same stars show up in the composite BVR images in fig. 5 of B15, although they are saturated. Thus, our study highlights UVIT's unique ability to resolve FUV-bright stars in the centre of sparsely populated stellar groups.

Our age estimates are similar to those estimated by B15 (∼25 Myr). Their catalogue includes OGLE-MBR-CL-0070 under its other name, BS 235. They adopted a metal-poor environment, $Z = 0.002$, but the upper limit of the uncertainty they assumed ($\Delta Z = +0.002$) agrees with our assumed value of $Z = 0.004$. B15 adopted $\mu_0 = 18.20 \pm 0.30$ mag, which agrees well with our best estimate for μ_0 based on the ($F148W$, $F148W-G$) CMD ($\mu_0 = 18.25 \pm 0.20$ mag), and it is within $\pm 1.5\sigma$ of that estimated using the (G, $BP-RP$) CMD ($\mu_0 = 18.75 \pm 0.20$ mag). Note that B15 employed visual isochrone fitting. The similarity of their results with ours validates the efficiency of our automated fitting algorithm for sparsely populated objects.

We estimated extinction values of $A_V = 0.20 \pm 0.02$ mag and $A_V = 0.41 \pm 0.02$ mag based on the (G, $BP-RP$) and ($F148W$, $F148W-G$) CMDs, respectively. We will discuss this discrepancy in Section 6. B15 used $E(B-V) \sim 0.0$ mag, implying zero extinction. Our method of parameter estimation is superior to visual fitting, which could be the reason for the discrepancy observed with respect to B15's results. We do not comment on whether this object is a genuine cluster. We suggest the need for a detailed kinematic analysis for such cases, which is beyond the scope of this work.

4.6 OGLE-MBR-CL-0075

OGLE-MBR-CL-0075 (Tile 3): The cluster's density enhancement is prominently visible in the *Gaia* spatial plot. The cluster's centre shows several FUV-bright stars and a distinct MS feature in the CMDs. The ages estimated from the ($F148W$, $F148W-G$) and (G, $BP-RP$) CMDs are similar ∼70 Myr, i.e. $\log \tau_G = 7.80 \pm 0.10$ and $\log \tau_{F148W} = 7.85 \pm 0.10$, respectively (see Figs 6 and 8).

As shown in fig. 5 of B15, the cluster is dominated by blue stars (some are saturated) in the composite BVR image. Note that B15 identifies this cluster by its other name, NGC 796. A. V. Ahumada et al. (2002) used an integrated spectrum to estimate an age of ∼6 Myr for this cluster. The presence of such blue (young) and bright stars along the line of sight could have led them to a biased estimate towards very young ages. Our estimations from both CMDs are consistent with those of B15 (42 Mr; $\log \tau = 7.63 \pm 0.19$) within $\pm 1\sigma$. Our age estimates are also consistent with that of G. I. Perren, A. E. Piatti & R. A. Vázquez (2017) (89 Myr; $\log \tau = 7.95 \pm 0.07$), within $\pm 1\sigma$, and agree within $\pm 2.5\sigma$ with A. E. Piatti et al. (2007) (112 Myr; $\log \tau = 8.05 \pm 0.10$). B15 investigated the discrepancy with A. E. Piatti et al. (2007) by analysing the Washington-band images used by A. E. Piatti et al. (2007). They found that those Washington-band images suffered from saturation owing to bright stars, which explains the difference with our values as well. The FUV-bright stars are distinctly visible and resolved in our UVIT images, and we did not observe any saturation (Fig. 2).

The extinction values, A_V, estimated from the (G, $BP-RP$) and ($F148W$, $F148W-G$) CMDs are markedly different, $A_V = 0.20 \pm 0.02$ mag and $A_V = 0.30 \pm 0.02$ mag, respectively. This discrepancy is driven by the colour separation between the MS stars, which extends up to ∼0.5 mag in the ($F148W$, $F148W-G$) CMDs, a separation that is twice as large as that observed in the optical CMDs. We present a discussion of this discrepancy in Section 6. The reddening values, $E(B-V)$, derived by B15 and G. I. Perren et al. (2017) are similar, 0.03 and 0.01 mag, respectively. Assuming $R_V = 3.1$ results in $A_V < 0.10$ mag. Our method of parameter estimation is more rigorous compared with visual fitting, which could be the reason for the discrepancy observed with B15. However, if we follow a similar justification as for BS 245, the order of magnitudes of extinction and the error in μ_0 values, for constant age, would imply that our extinction estimates are similar to those of B15.

The μ_0s estimated using the (G, $BP-RP$) and ($F148W$, $F148W-G$) CMDs are 18.50 ± 0.20 and 18.25 ± 0.20 mag, respectively, consistent within $\pm 1\sigma$. These values agree with the estimates of B15 ($\mu_0 = 18.04 \pm 0.28$ mag) but disagree with those of G. I. Perren et al. (2017) ($\mu_0 = 19$ mag). The reason for this difference is that G. I. Perren et al. (2017) adopted a μ_0 grid ranging from 18.86 to 19.06 mag, which did not reach LMC-like distances. Our study confirms that this cluster is indeed younger than 100 Myr, that it is located at an LMC-like distance and that it hosts several FUV-bright stars near the cluster centre.

4.7 L 114

L 114 (Tile 4): The cluster is observed as a prominent density clump in its *Gaia* spatial distribution, as well as in the UVIT FUV image. The cluster region hosts a prominent MS (see Figs 6 and 8). We estimate an age of ∼63 Myr ($\log \tau = 7.80 \pm 0.10$). Our age estimations validated using both of our usual CMDs are in complete agreement with one another. Our estimates are

younger compared to A. E. Piatti et al. (2007)'s (140 Myr; $\log \tau = 8.15 \pm 0.15$), who used $(T_1, C - T_1)$ CMDs and isochrones from the Padova group and assumed $Z = 0.004$ with $\mu_0 = 18.77$ mag. The error in their age is +60 Myr and −40 Myr, which suggests that our ages agree within $\pm 2\sigma$ of their values.

Our $\mu_0 = 18.00 \pm 0.20$ mag and 18.25 ± 0.20 mag estimates from both CMDs are consistent with one another and smaller compared with A. E. Piatti et al. (2007). The reddening ($E(B-V)$) estimated by A. E. Piatti et al. (2007) is 0.04 mag, which translates to an extinction of 0.12 mag. The extinction estimated by us is greater than their values. Also, the value of A_V estimated from the ($F148W$, $F148W-G$) CMD is higher (0.41 ± 0.02 mag) than that derived from the (G, $BP - RP$) CMD (0.32 ± 0.02 mag), deviating by $\pm 5\sigma$. We will present a discussion of this discrepancy between the two estimated extinctions in this study in Section 6. It is to be noted that the value of μ_0 assumed by A. E. Piatti et al. (2007) was adopted to maintain consistency across all SMC clusters they had analysed, and the reddening value estimated by them by interpolating reddening maps in literature. The age fits to CMDs are carried out using these values. In comparison, our fitting method is statistically more rigorous where the parameters (age, μ_0, and extinction) are estimated from a grid of physically possible values.

Moreover, we also fit the three brightest stars observed in the CMD, which are located within the average cluster radii (0.65 arcmin) mentioned by B08. These three stars survived the parallax and pm cuts, and hence were treated as potential cluster members. The CMDs of A. E. Piatti et al. (2007) possibly missed these bright stars because they considered a smaller cluster radii (≈ 25 arcsec). In the past, A. V. Ahumada et al. (2002) had estimated an age of 5.6 ± 0.5 Gyr for this cluster using an integrated spectrum and by comparison with template spectra. Equivalent widths were used to estimate the ages. Generally speaking, age estimations based on integrated spectra are not as accurate, and in this case, the inaccuracy may be owing to the bimodal behaviour of the Balmer-line equivalent widths (A. E. Piatti et al. 2007). Overall, our results suggest that L 114 could be younger than 100 Myr and is located at a distance similar to that of the LMC, or even closer.

5 SPECTRAL ENERGY DISTRIBUTION OF UV-BRIGHT MS STARS

To analyse the UV-bright MS stars, we selected the MS stars from the ($F148W$, $F148W-G$) CMDs. We used stars with $F148W$ magnitudes brighter than 19 mag. We compared the observed magnitudes with PARSEC models. For all clusters, this luminosity limit corresponds to masses $\geq 2.5 M_\odot$, that is, typically the lower limit of B-type stellar masses. We checked various archives (e.g. ESO, NOAO) but did not find spectroscopic data of MS stars in our observed UVIT fields, except for three stars which had already been analysed by V. Ramachandran et al. (2021). We have used the stellar SEDs to estimate some of the fundamental parameters ($T_{\rm eff}$ and $\log g$) of UV-bright MS stars, which could be OB-type stars. We used the widely accepted TLUSTY stellar atmospheric models for OB stars (T. Lanz & I. Hubeny 2007) to fit model spectra to a set of photometric magnitudes: UV (UVIT FUV and *GALEX* FUV & NUV), optical (*GaiaG*, *BP* and *RP*) and NIR (VMC: Y, J, K_s, or 2MASS if VMC data were unavailable). SED generation and fitting of TLUSTY synthetic spectra was achieved using the virtual observatory SED analyser (VOSA[2]; A. Bayo et al. 2008). We selected the entire range of $T_{\rm eff}$ and $\log g$ values as suggested for TLUSTY models, i.e. 15 000–55 000 K and 1.75–4.75 dex, respectively. Chemical abundances inferred from B-type stars and the ISM gas phase suggest a mean metallicity of $Z/Z_\odot < 0.1$ in the Bridge (V. Ramachandran et al. 2021). R. A. P. Oliveira et al. (2023) highlighted the existence of star clusters with metallicities [Fe/H] > -0.5 dex and counterparts with [Fe/H] < -0.6 dex. Thus, we adopted metallicity ($Z/Z_\odot$) values up to 0.20 for the TLUSTY models in VOSA. This typically covers SMC-like metallicity range. We used A_V and distance values from our analysis as mentioned in Section 3.4. These values are necessary to scale the model spectra to the observed flux distribution. We used a minimum of eight photometric filters per star to generate their SEDs.

VOSA performs multiple iterations by varying $T_{\rm eff}$ and $\log g$, to minimize reduced χ^2 ($\chi^2_{\rm red}$) to find the best-fitting spectra to the observed flux distribution. $\chi^2_{\rm red} = \chi^2/(N - {\rm n}_p)$, where N is the number of photometric points and n_p is the number of fitted parameters used in the model. (N–n_p) are the degrees of freedom associated with the χ^2 test. However, in cases where photometric uncertainties are very small, the standard $\chi^2_{\rm red}$ statistic can yield large values even when the SED appears visually well-fitted. To mitigate this effect, VOSA computes the visual goodness of fit (Vgf_b) by imposing a minimum uncertainty of 10 per cent of the observed flux in the $\chi^2_{\rm red}$ formula. Following previous studies (A. Rebassa-Mansergas et al. 2021; P. K. Nayak, A. Ganguly & S. Chatterjee 2024), we adopt $\mathrm{Vgf}_b < 15$ as the criterion for well-fitted SEDs. We found 51 stars in the seven objects, for which we found a match with *GALEX* FUV & NUV, *Gaia*, and VMC/2MASS. We did not have FUV data from *GALEX* available for BS 245, OGLE-MBR-CL-0084 and OGLE-MBR-CL-0030. We used the 2MASS catalogue in NIR for the cluster OGLE-MBR-CL-0075 due to the unavailability of VMC data. Except for two stars (one in OGLE-MBR-CL-0075 and one in OGLE-MBR-CL-0030), all the other stars show $\mathrm{Vgf}_b < 15$ and are considered as well-fitted SEDs.

Below, we present a summary of the SED analysis of MS stars in our seven objects, along with the parameters of the hottest stars detected in our analysis. The table summarizing the parameters of the hot MS stars and their SEDs are presented in Appendices A and C, respectively. Best-fitting SEDs of two stars from BS 245 are presented in Fig. 10. TLUSTY atmospheric models (grey lines) are fitted to the observed fluxes (cyan points with blue error bars), assuming a single-star configuration. The red points correspond to the model-predicted fluxes from the best-fitting synthetic spectra. *Gaia*-DR3 source ID, the values of A_V, χ^2_{red}, and Vgf_b are mentioned on top of panels. Best-fitting $T_{\rm eff}$ and $\log g$ values are mentioned in the legend. The lower panel of each plot displays the fractional residual flux ($f_{\rm residue}$) in each band, defined as the fractional difference between the observed and model-predicted flux, $f_{\rm residue} = \frac{F_{\lambda,\rm obs} - F_{\lambda,\rm model}}{F_{\lambda,\rm obs}}$, where F_λ is the flux at wavelength λ, and the subscripts 'obs' and 'model' refer to the observed and best-fitting model fluxes, respectively. The blue and red dashed lines mark residual levels of 50 and 100 per cent, respectively, while the black line indicates zero residual. The good agreement between the cyan and red points, together with residuals below 50 per cent across all bands, demonstrates that the SEDs are well-fitted. Note that with UVIT, we were able to resolve the hottest

[2] http://svo2.cab.inta-csic.es/theory/vosa/helpw4.php?otype=star&action=help

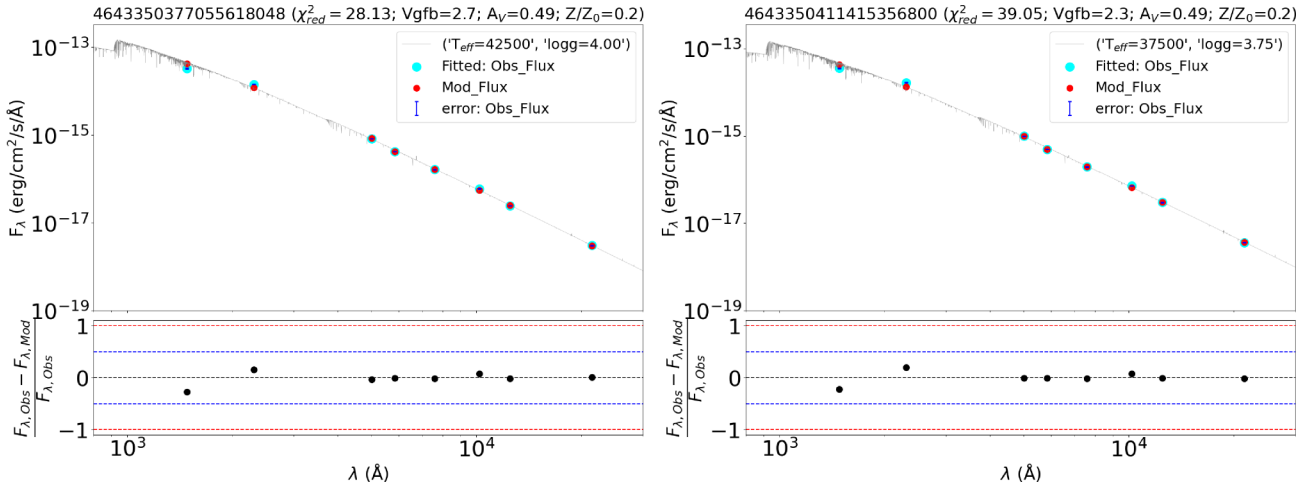

Figure 10. Well-fitted SEDs of two stars in BS 245. Left: $T_{\rm eff}$ = 42, 500 K ($\log g = 4.0 \pm 0.12$ dex) and (right) 37 500 K ($\log g = 3.75 \pm 0.12$ dex). *Gaia*-DR3 source ID, the values of A_V, χ^2_{red}, and Vgf_b are mentioned on top of each panel. TLUSTY atmospheric models (grey line) were fitted to the observed fluxes from UV to NIR (cyan points with blue errors), assuming a single star. The red points indicate the expected model fluxes from the best-fitting synthetic spectra. In the bottom panel of each plot, fractional residual fluxes are shown for different bands. The blue and red dashed lines indicate 50 and 100 per cent residual flux, respectively, while the black line denotes zero residual. The close agreement between the cyan and red data points, along with residuals below 50 per cent in all bands, demonstrates a well-fitted SED.

stars in crowded cores without any saturation, except for one star in OGLE-MBR-CL-0075.

(i) BS 245: We found four stars with cross-matched data from UVIT, *Gaia,* and VMC. Two hottest stars have $T_{\rm eff} = 42\,500 \pm 1250$ K ($\log g = 4.0 \pm 0.1$ dex) and $T_{\rm eff} = 37\,500 \pm 1250$ K ($\log g = 3.75 \pm 0.1$ dex): see Fig. 10. The other two stars are characterized by $T_{\rm eff} = 16\,000 \pm 500$ K and $T_{\rm eff} = 18\,000 \pm 500$ K, with $\log g = 2.5 \pm 0.15$ dex and 2.25 ± 0.12 dex, respectively (see Table A1, Appendix A). The remaining SEDs are shown in Fig. C1 (Appendix C).

(ii) OGLE-MBR-CL-0084: We found two stars with $T_{\rm eff} = 23\,000 \pm 500$ K ($\log g = 2.5 \pm 0.1$ dex) and $T_{\rm eff} = 24\,000 \pm 500$ K ($\log g = 2.75 \pm 0.1$ dex). Although we detected 11 MS stars in the (F148W, F148W−*G*) CMD, we managed to retrieve only two stars with cross-matched data from UVIT, *Gaia*, and VMC. The stellar parameters are listed in Table A1 (Appendix A). The corresponding SEDs are shown in Fig. C2 (Appendix C).

(iii) OGLE-MBR-CL-0030: This cluster contains only four bright MS stars. We found only one star with cross-matched values among UVIT, *Gaia* and VMC data. However, the number of photometric data points are less than eight and the SED fit gives higher Vgf_b value (79.2), as shown in Fig. C3 (Appendix C). Therefore, we are unable to provide reliable stellar parameters for this star. The stellar parameters are listed in Table A1 (Appendix A).

(iv) OGLE-MBR-CL-0070: There are three UV-bright MS stars. One has $T_{\rm eff} = 32\,500 \pm 1250$ K and $\log g = 3.5 \pm 0.1$ dex: see Fig. 11. The other two have $T_{\rm eff} = 18\,000 \pm 500$ K ($\log g = 2.5 \pm 0.1$ dex) and $T_{\rm eff} = 23\,000 \pm 500$ K ($\log g = 3.2 \pm 0.1$ dex). The stellar parameters are listed in Table A2 (Appendix A). Their SEDs are shown in Fig. C4 (Appendix C).

(v) OGLE-MBR-CL-0026: Three of nine UV-bright stars in this cluster have $T_{\rm eff}$ between 30 000 K and 32 500 K. Two stars are the hottest, with $T_{\rm eff} = 32500 \pm 1250$ K and $\log g$ between 3.5 ± 0.1 and 3.75 ± 0.1 dex: see Fig. 11. All remaining SEDs are shown in Figs C5 and C6 (Appendix C), where five of the nine stars have temperatures between 24 000 K and 29 000 K (see Table A2, Appendix A). One star has $T_{\rm eff} = 17000 \pm 500$ K. All stars have $\log g$ ranging between 2.25 ± 0.1 and 3.75 ± 0.1 dex.

(vi) For OGLE-MBR-CL-0075, we identified 46 MS stars brighter than FUV mag = 19. Eight were cross-matched with *GALEX* data. VMC data were unavailable for this cluster; therefore, we selected the 2MASS point source catalogue and found six stars with cross-matched *J*-, *H*-, and $K_{\rm s}$-band magnitudes. However, the 2MASS data have a shallower photometric depth than the VMC survey; hence, for most of the $K_{\rm s}$ band, the data are unreliable (the error value is NULL) for UV-bright MS stars. Of these six stars, five stars have Vgf_b values <15, while one star has very high Vgf_b value of 103, suggesting that the SED fit is not reliable. Hence, we provide reliable stellar parameters for five stars in this cluster (see Table A3, Appendix A). One star is found to have a temperature in excess of 20 000 K: $T_{\rm eff} = 21\,000 \pm 500$ K ($\log g = 2.25 \pm 0.1$ dex). All SEDs are shown Fig. C7 (Appendix C), including the poorly-fitted SED (bottom right figure).

(vii) For L 114, we are able to estimate parameters for 26 MS stars. The highest temperature measured is $T_{\rm eff} = 24\,000 \pm 500$ K and $\log g = 2.5 \pm 0.1$. There are nine stars with $T_{\rm eff}$ between $20,000 \pm 500$ K and 22000 ± 500 K. The surface gravity for these stars ranges between $\log g = 2.25 \pm 0.1$ and 2.75 ± 0.1 dex. The remaining 13 stars have $T_{\rm eff}$ between 15 000 and 18 000 $\pm$500 K, with $\log g$ ranging from 1.75 ± 0.1 to 2.75 ± 0.1 dex. The stellar parameters are listed in Table A4 (Appendix A). All SEDs are shown in Figs C8–C12 (see Appendix C).

6 DISCUSSION

Three of the seven cluster candidates are confirmed star clusters: L 114, OGLE-MBR-CL-0075, and BS 245. Three objects, listed as cluster candidates by M. Sitek et al. (2017) have been parametrized for the first time in this study: OGLE-MBR-CL-0026, OGLE-MBR-CL-0030, and OGLE-MBR-CL-0084. The $\chi^2_{\rm f}$ values estimated from both CMDs are $\lesssim 1$ for OGLE-MBR-CL-0084 and OGLE-MBR-CL-0070 compared with OGLE-MBR-CL-0026 and OGLE-MBR-CL-0030, which suggests better isochrone

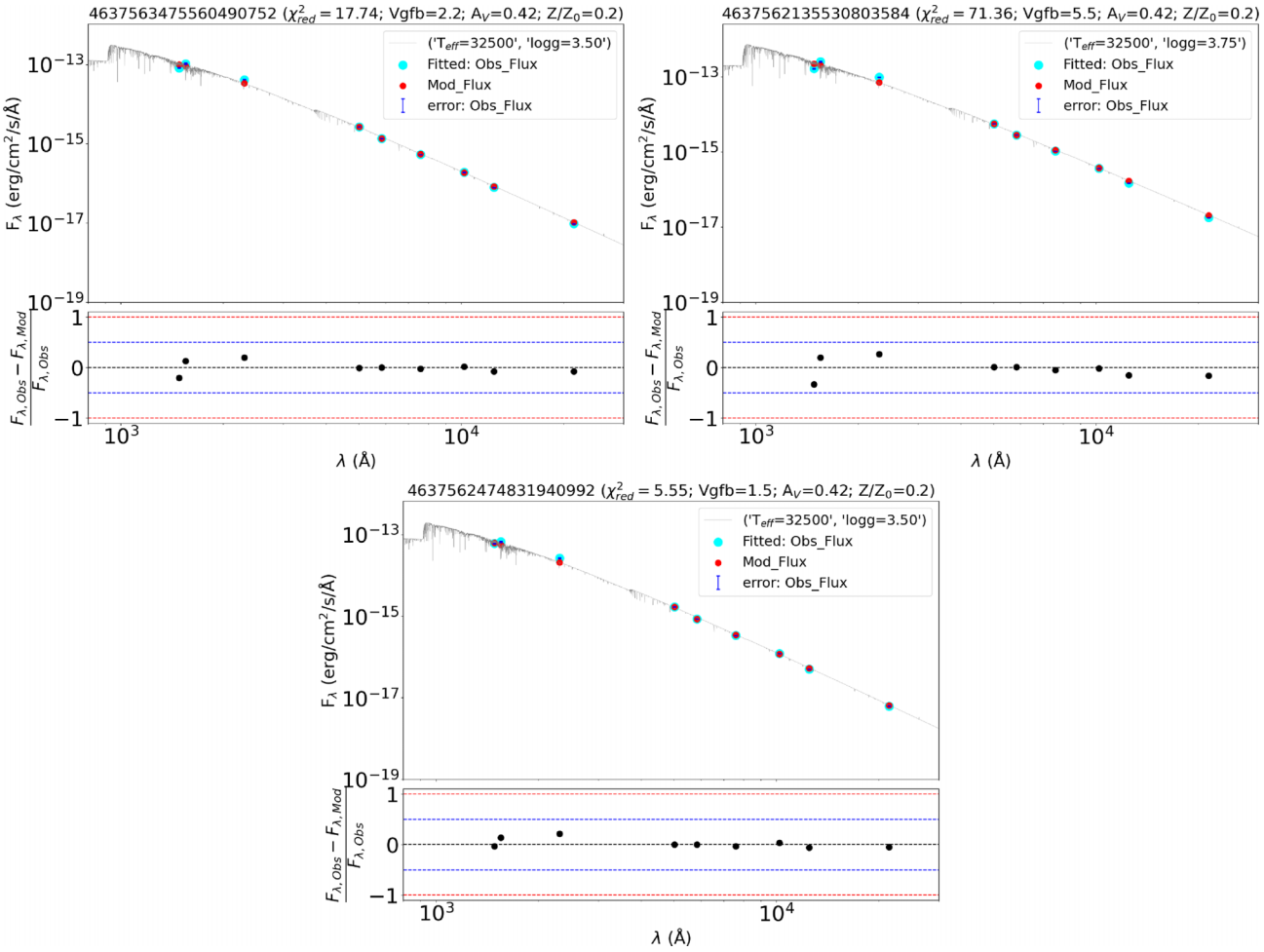

Figure 11. *Top left:* OGLE-MBR-CL-0070: SED of the hottest star with $T_{\rm eff}$ = 32, 500 K ($\log g = 3.5 \pm 0.12$ dex). *Top right and Bottom:* OGLE-MBR-CL-0026: SED of two stars with similar $T_{\rm eff}$ = 32, 500 K (but for $\log g = 3.75 \pm 0.12$ and 3.5 ± 0.12 dex). TLUSTY atmospheric models were fitted to the SEDs assuming single stars, and (bottom) residuals for each star are shown.

fits to the MS for the former cases. The FUV images of OGLE-MBR-CL-0026 and OGLE-MBR-CL-0084 show seven to eight FUV-bright stars in the cluster region, whereas OGLE-MBR-CL-0030 and OGLE-MBR-CL-0070 lack such stars (or contain only one or two). Since OGLE-MBR-CL-0084 satisfies both criteria, we suggest that it is a star cluster, as also suggested by M. Sitek et al. (2017). For the remaining three objects (OGLE-MBR-CL-0070, OGLE-MBR-CL-0026, and OGLE-MBR-CL-0030), it is difficult to verify their physical reality. It is possible that they fall into the very low-mass category ($< 800\,M_\odot$) of MC star clusters (P. K. Nayak et al. 2018) or they may be associations. Further confirmation of their nature would require spectroscopic and kinematic analysis, which is beyond the scope of this study.

With the help of UVIT, we resolved the individual UV-bright MS stars in these seven stellar clusters and aggregates and identified them as four clusters and three possible clusters/associations. We considered a (thrice) larger radius of these objects than adopted in Bica's catalogue. We removed Galactic contamination based on initial pm and parallax cuts. At the distances to the MCs, the errors in *Gaia* pm measurements cannot help distinguish between field stars in the Bridge and cluster members. Hence, we defined cluster members as stars above the 50th percentile from the KDE plot of the pm plane, since they are located within the clumpiest part of the distribution. It is possible that a few stars in the CMDs are non-members, but there is no better way to distinguish between a cluster and a non-cluster member in the absence of kinematic (spectroscopic) data. Note that the primary motivation of this work was not to accurately identify all cluster members. The definition of our cluster members is optimized to populate the MSs of the CMDs, allowing us to apply our automated technique for cluster parameter estimation. This is based on the assumption that UV-bright stars may also be dispersed outside the radii defined in Bica's catalogue. In fact, we validated that assumption by checking the spatial distribution of FUV-bright stars around the cluster centres in the UVIT images.

Parametrization of all seven objects was carried out using a systematic automated technique applied to two different CMDs, (G, $BP - RP$) and ($F148W$, $F148W{-}G$). Ages estimated based on the ($F148W$, $F148W{-}G$) CMDs are consistent with those estimated using the (G, $BP - RP$) equivalents within ± 1–2σ (where $\sigma = 0.10$ dex in age). Overall, our age estimations indicate that all seven objects range between 15 and 70 Myr, i.e. they are younger than 100 Myr. The error in extinction (± 0.02 mag in A_G, and ± 0.02 mag in $A_{\rm F148W}$), when added to the error in μ_0 – ± 0.20 mag, implies that the apparent magnitude of the MS stars could vary by $\approx \pm 0.22$ mag. This implies that the maximum uncertainty in our age estimates could be ± 0.20 dex.

The 14 star clusters studied by B15 lie between RA = 29 to 37° and from Dec. = −76 to −73°. They span a relatively larger spatial area of the Bridge than the objects inspected in this study (RA = 27.5° to 37.5° and Dec. = −74.5 to −73.5°). B15 suggested a μ_0 range of 18.00–18.40 mag, with a typical uncertainty of ±0.30 mag, based on $(V, V-R)$ CMDs obtained with the 4 m SOAR telescope. Of the two CMDs we analysed here, we compared the μ_0 values estimated using *Gaia* CMDs with B15, since the *VR* bands lie within the wavelength regime of the *GaiaG*, *BP* and *RP* passbands. The distance modulus for the four confirmed clusters are $\mu_0 = 18 \pm 0.20$ mag (L 114), 18.50 ± 0.20 mag (OGLE-MBR-CL-0075), 18.50 ± 0.20 mag(BS 245), and 18 ± 0.20 mag (OGLE-MBR-CL-0084). The range of μ_0 (18.00–18.50 mag) is consistent with the range of values found by B15. Moreover, it strengthens the evidence of distance variations in the Bridge region analysed in this paper. Our results agree with the suggestion of B15 that this portion is located closer to us than the typical SMC μ_0 (R. de Grijs & G. Bono 2015). The uncertainties estimated by B15 are slightly larger than those obtained here.

We used $A_{\rm FUV}/A_V = 2.65$ and $A_G/A_V = 0.84$ to convert A_G and $A_{\rm FUV}$ to extinction in the V band (A_V). The conversions are based on the J. A. Cardelli, G. C. Clayton & J. S. Mathis (1989) and J. E. O'Donnell (1994) extinction curve with $R_V = 3.1$.. To avoid confusion, we refer to the estimated extinction derived from the $(F148W, F148W-G)$ CMD as $A_{V\rm fuv}$ and to that from the $(G, BP-RP)$ CMD as A_{Vg}. The central tendencies of $A_{V\rm fuv}$ for the seven objects are: mean = 0.34 mag, standard deviation = 0.13 mag, median = 0.41 mag; for A_{Vg}: mean = 0.24 mag, standard deviation = 0.10 mag, median = 0.20 mag. Overall, the estimated extinction based on the $(F148W, F148W-G)$ CMDs is higher than that from the $(G, BP-RP)$ CMDs. The relative difference in extinction between $A_{V\rm fuv}$ and A_{Vg}, varies from 32 to 71 per cent. This difference is also observed in confirmed clusters (L 114, BS 245, OGLE-MBR-CL-0075, and OGLE-MBR-CL-0084), where it is ≈ 30 per cent. The extinction values resulting from studies of SMC star clusters by D24 (their fig. 6) show that A_G ranges from 0.28 to 0.48 mag along sightlines towards the Bridge region. Our A_G values are in the same range as those of D24.

The difference in extinction estimates based on UV–optical and optical-only CMDs suggests that a larger number of UV photons are being absorbed and scattered in the UV compared with optical photons. Recent studies of young MC star clusters have suggested that dimming of UV radiation is a property of young (≲200 Myr-old) clusters. A. P. Milone et al. (2023) suggested that such MS stars occupy the bluer part of the UV–optical CMD. They are distinctly observed as a separate sequence in *Hubble Space Telescope* colour–colour diagrams – $(F225W-F336W)$ versus $(F336W-F814W)$ or $(F275W-F336W)$ versus $(F336W-F814W)$. The authors suggested that they may be Be stars, where the UV dimming is caused by a combination of dusty circumstellar material and the star's orientation with respect to the line of sight. We do not discard the possibility that the MS stars in our young objects have dusty circumstellar discs, which may cause enhanced extinction of UV photons. However, validation is beyond the scope of this work.

The $(F148W-G)$ colour width is generally larger than the $(BP-RP)$ colour spread. This is prevalent in our CMDs. Our automated method for estimating parameters selects extinction from a grid of values and simultaneously explores a parameter space of ages and μ_0 values. Age fitting along the magnitude axis is subject to a degeneracy if trying to select between extinction and μ_0 values, whereas for the colour axis the algorithm attempts to optimize the $A_{\rm FUV}$ minus A_G values so as to estimate a $\chi^2_{\rm red}$ value. In general, the number of stars in our CMDs is smaller than expected for rich MC star clusters. It is possible that the discrepancy observed in extinction is owing to statistical fluctuations driven by the small number of stars available, the larger colour spread inherent to UV–optical CMDs compared with optical-only CMDs and the degeneracy between extinction and μ_0. We particularly note an inconsistency pertaining to the extinction estimation of one object, OGLE-MBR-CL-0030. The estimated values of $A_{\rm FUV}$ and A_G are almost similar, leading to an estimation of smaller values for the extinction based on the $(F148W, F148W-G)$ CMDs compared with the $(G, BP-RP)$ CMDs.

We have used multiwavelength photometric catalogues in the UV (UVIT and *GALEX*), optical (*Gaia*), and NIR (VMC/2MASS) to estimate the stellar properties of the FUV-bright MS stars in all seven target objects. The high-resolution UVIT FUV images in Figs 1 and 2 show that we have been able to resolve individual stars. This paper emphasizes UVIT's ability to resolve individual stellar populations in crowded regions (i.e. in open cluster-like objects) located at LMC/SMC distances. The only other study thus far that has tested UVIT's ability to resolve such stellar populations in star clusters was done for the SMC cluster Kron 3 by P. K. Nayak et al. (2021).

SED fits to multiwavelength photometric fluxes were performed using the VOSA, using TLUSTY models. The mean $T_{\rm eff}$ of the distribution of the 51 hot stars in all seven objects is 21 696 K, with a standard deviation of 7661 K. Seven of the 51 stars (∼13 per cent) have $T_{\rm eff} \geq 29,357$ K (mean $T_{\rm eff}$ plus the standard deviation); they could be late O-type stars. OGLE-MBR-CL-0075 could host a large number of hot stars similar to L 114, but SEDs are presented only for stars with 2MASS NIR data available. We may have missed the faint-UV stars while cross-matching UVIT and 2MASS data. This is because of the shallow photometric depth of the 2MASS data. Thus, it is possible that the fraction of late O-type stars could be smaller than 17 per cent.

The mean $\log g = 2.57$ dex with a standard deviation of 0.61 dex for all 51 stars. The range of values for $\log g$ is indicative of typical MS stars. However, the values are smaller compared to the values for MS stars in the Milky Way (usually between 3 and 4). A linear fit to the $\log g$ versus $T_{\rm eff}$ data suggests a slope of $\approx 1 \times 10^{-4}$, with a correlation coefficient of 0.92. We checked the VOSA for variations in extinction and μ_0, but variations in $T_{\rm eff}$ and $\log g$ values were within their corresponding ± 3σ ranges (500–1250 K and 0.1 dex, respectively). We also verified that the selection of Kurucz instead of TLUSTY atmospheric models does not affect our estimation of $T_{\rm eff}$ and $\log g$, i.e. the variations are within ± 1σ, thus emphasizing that these estimations are model-independent.

Note that our sample of hot MS cluster stars does not include the three O-type stars discovered in the Bridge by V. Ramachandran et al. (2021). Those authors used VLT/FLAMES data to estimate the stellar parameters of three O-type stars (with ranges in $T_{\rm eff}$ == 33 000–34 000 K, $\log g = 3.5$–4.0 dex and masses in the range of 18–19$M_\odot$) and multi-epoch observations to find that all three were binaries. The metallicity estimations suggested that one of them was LMC-like, whereas the other two were SMC-like. We do not have access to the spectra of the hot MS stars analysed in this paper. SED fits suggest the presence of five stars with ranges in $T_{\rm eff} = 32\,500$–$42\,500$ K and $\log g = 3.5$–4.0 dex, similar to that of the three O-type stars studied by V. Ramachandran et al. (2021). They are found in cluster BS 245, and in stellar aggregates OGLE-MBR-CL-0070 and OGLE-MBR-CL-0026. These, and the remaining hot MS stars, should be studied spectroscopically in

future to accurately estimate their stellar parameters, including $T_{\rm eff}$, log g, elemental abundances and binarity.

7 SUMMARY

In this paper, we have analysed the first high-resolution FUV ($F148W$) images of seven star cluster candidates in the Magellanic Bridge using the UVIT on *AstroSat*. The star targets are located in four UVIT fields, spanning a region of approximately 3 deg^2. The FUV images show UVIT's unique ability to resolve individual stellar populations at the distance of the MCs within crowded fields. This enabled the estimation of the parameters of UV-bright star clusters, inspection of their validation using CMDs, and stellar parameter estimation of individual hot MS stars within them.

CMD analysis based on UVIT FUV data and *Gaia* DR3 suggests four confirmed star clusters: L 114, OGLE-MBR-CL-0075, BS 245, and OGLE-MBR-CL-0084. The other objects may be OB associations or clusters subject to dissolution owing to the tidal forces between the Clouds, including OGLE-MBR-CL-0026, OGLE-MBR-CL-0030, and OGLE-MBR-CL-0070. This is contrary to their categorization as cluster candidates in B08's (or B20's) catalogue.

Our age estimations of all seven objects based on the ($F148W$, $F148W-G$) and (G, $BP-RP$) CMDs are in mutual agreement. The estimated ages range from 15 to 70 Myr, i.e. younger than 100 Myr, for all objects studied. Note that three objects have been parametrized for the first time in this paper, including OGLE-MBR-CL-0026, OGLE-MBR-CL-0030, and OGLE-MBR-CL-0084.

The estimated μ_0 range and mean μ_0 (18.43 mag, standard deviation: $\pm$0.17 mag) emphasize that the spatial region investigated lies closer to us, compared with the SMC, with the farthest distance similar to the LMC's μ_0. This validates previous results by B15, who inspected a larger set of clusters across a similar but more extended spatial region of the Bridge.

For the first time, we present SED modelling of young MS stars in these clusters by combining precise FUV photometric data from UVIT with NUV data from *GALEX*, optical data from *Gaia* and NIR data from the VMC survey. Where VMC was unavailable, we used 2MASS data. Our analysis of hot MS stars is limited to objects brighter than 19.0 mag in the FUV for all seven objects. The SED analysis suggests the presence of five hot MS stars with ranges in $T_{\rm eff}$ = 32 500–42 500 K and log g = 3.5–4.0 dex: two stars in BS 245, one star in OGLE-MBR-CL-0070 and two stars in OGLE-MBR-CL-0026. The $T_{\rm eff}$ and log g ranges are similar to those of the three O-type stars discovered by V. Ramachandran et al. (2021). However, validation requires detailed spectroscopic analysis. We release a photometric catalogue of UVIT-detected sources associated with our seven target objects as supplementary material. The catalogue contains stars within approximately ten times the radius of each stellar aggregate (as mentioned in the literature), in the following sequence: RA, Dec, F148W magnitude (AB system), error in $F148W$ magnitude and sharpness (from PSF photometry). This catalogue could be used to inspect the surrounding field region of each stellar aggregate, and cross-matched with publicly available data for spectroscopic and binarity investigations.

ACKNOWLEDGEMENTS

We thank the anonymous referees for their feedback, which helped improve the quality of the manuscript. SC acknowledges the support of Ahmedabad University start-up grant (URBSASI24A4) to support this research. PKN acknowledges the support from the Centro de Astrofísica y Tecnologías Afines (CATA) fellowship via grant Agencia Nacional de Investigaciõn Desarrollo (ANID), BASAL FB210003. This research is based on observations using the UVIT (Proposal ID: A09_012, PI: S. Choudhury) on the *AstroSat* mission, which are archived at the Indian Space Science Data Centre (ISSDC). This work has made use of *Gaia* DR3 from the European Space Agency (ESA) mission *Gaia* (https://www.cosmos.esa.int/gaia), processed by the *Gaia* Data Processing and Analysis Consortium (DPAC; https://www.cosmos.esa.int/web/gaia/dpac/consortium). Funding for the DPAC has been provided by national institutions, in particular the institutions participating in the *Gaia* Multilateral Agreement. The VMC (PI: M.R.L. Cioni) data used in this work are based on data products created from observations collected at the European Organisation for Astronomical Research in the Southern Hemisphere under ESO programme 179.B-2003. The PSF data of VMC (version 4) were obtained from the ESO Science Archive Facility, with DOI:10.18727/archive/64. This publication makes use of VOSA, developed under the Spanish Virtual Observatory project supported by the Spanish MICINN through grant A2011-24052. The authors acknowledge PYTHON packages used in this work, like NUMPY (C. R. Harris et al. 2020), MATPLOTLIB (J. D. Hunter 2007) and SCIPY (P. Virtanen et al. 2020).

DATA AVAILABILITY

UVIT data for all four tiles used in this study are available in the AstroSat data archive[3] The PSF photometric catalogue of all the MS stars for each of the seven objects is made available. Further, we provide a consolidated table of stellar parameters of all 51 MS stars, along with their *Gaia* IDs and the stellar aggregate/cluster each star belongs to.

REFERENCES

Ahumada A. V., Clariá J. J., Bica E., Dutra C. M., 2002, A&A, 393, 855
Bayo A., Rodrigo C., Barrado Y Navascués D., Solano E., Gutiérrez R., Morales-Calderón M., Allard F., 2008, A&A, 492, 277
Besla G., Kallivayalil N., Hernquist L., van der Marel R. P., Cox T. J., Kereš D., 2012, MNRAS, 421, 2109
Bianchi L., Conti A., Shiao B., 2014, Adv. Space Res., 53, 900
Bica E., Bonatto C., Dutra C. M., Santos J. F. C., 2008, MNRAS, 389, 678 (B08)
Bica E., Santiago B., Bonatto C., Garcia-Dias R., Kerber L., Dias B., Barbuy B., Balbinot E., 2015, MNRAS, 453, 3190 (B15)
Bica E., Westera P., Kerber L. D. O., Dias B., Maia F., Santos J. F. C. Jr, Barbuy B., Oliveira R. A. P., 2020, AJ, 159, 82 (B20)
Bressan A., Marigo P., Girardi L., Salasnich B., Dal Cero C., Rubele S., Nanni A., 2012, MNRAS, 427, 127
Cardelli J. A., Clayton G. C., Mathis J. S., 1989, ApJ, 345, 245
Casetti-Dinescu D. I., Vieira K., Girard T. M., van Altena W. F., 2012, ApJ, 753, 123
Chen C. H. R. et al., 2014, ApJ, 785, 162
Choudhury S., Subramaniam A., Piatti A. E., 2015, AJ, 149, 52
Cioni M. R. L. et al., 2011, A&A, 527, A116
Crampton D., Greasley J., 1982, PASP, 94, 31
de Grijs R., Bono G., 2015, AJ, 149, 179
de Grijs R., Wicker J. E., Bono G., 2014, AJ, 147, 122

[3]https://astrobrowse.issdc.gov.in/astro_archive/archive/Home.jsp

Dhanush S. R., Subramaniam A., Nayak P. K., Subramanian S., 2024, MNRAS, 528, 2274 (D24)
Gaia Collaboration, 2023, A&A, 674, A1
Girish V., Tandon S. N., Sriram S., Kumar A., Postma J., 2017, Exp. Astron., 43, 59
Harris C. R. et al., 2020, Nature, 585, 357
Harris J., 2007, ApJ, 658, 345
Hota S., Subramaniam A., Nayak P. K., Subramanian S., 2024a, AJ, 168, 255
Hota S., Subramaniam A., Dhanush S. R., Cioni M.-R. L., Subramanian S., 2024b, MNRAS, 532, 322
Hunter J. D., 2007, Comput, Sci. Eng., 9, 90
Irwin M. J., Kunkel W. E., Demers S., 1985, Nature, 318, 160
Lamb J. B., Oey M. S., Segura-Cox D. M., Graus A. S., Kiminki D. C., Golden-Marx J. B., Parker J. W., 2016, ApJ, 817, 113
Lanz T., Hubeny I., 2007, ApJS, 169, 83
Mackey A. D., 2009, in Mamajek E. E., Soderblom D. R., Wyse R. F. G. eds, Proc. IAU Symp. 258, The Ages of Stars. p. 275
Martin D. C. et al., 2005, ApJ, 619, L1
Massey P., Lang C. C., Degioia-Eastwood K., Garmany C. D., 1995, ApJ, 438, 188
Milone A. P. et al., 2023, A&A, 672, A161
Muller E., Staveley-Smith L., Zealey W., Stanimirović S., 2003, MNRAS, 339, 105
Murray C. E., Peek J. E. G., Di Teodoro E. M., McClure-Griffiths N. M., Dickey J. M., Dénes H., 2019, ApJ, 887, 267
Nayak P. K., Subramaniam A., Choudhury S., Indu G., Sagar R., 2016, MNRAS, 463, 1446
Nayak P. K., Subramaniam A., Choudhury S., Sagar R., 2018, A&A, 616, A187
Nayak P. K. et al., 2021, MNRAS, 503, 5291
Nayak P. K., Ganguly A., Chatterjee S., 2024, MNRAS, 527, 6100
Nidever D. L. et al., 2017, AJ, 154, 199
O'Donnell J. E., 1994, ApJ, 422, 158
Oliveira R. A. P. et al., 2023, MNRAS, 524, 2244
Perren G. I., Piatti A. E., Vázquez R. A., 2017, A&A, 602, A89
Piatti A. E., Sarajedini A., Geisler D., Gallart C., Wischnjewsky M., 2007, MNRAS, 382, 1203
Piatti A. E., de Grijs R., Rubele S., Cioni M.-R. L., Ripepi V., Kerber L., 2015, MNRAS, 450, 552
Pietrzynski G., Udalski A., 2000, AcA, 50, 355
Postma J., Hutchings J. B., Leahy D., 2011, PASP, 123, 833
Postma J. E., Leahy D., 2017, PASP, 129, 115002
Ramachandran V., Oskinova L. M., Hamann W. R., 2021, A&A, 646, A16
Rebassa-Mansergas A. et al., 2021, MNRAS, 506, 5201
Sitek M. et al., 2016, AcA, 66, 255
Sitek M. et al., 2017, AcA, 67, 363
Skowron D. M. et al., 2014, ApJ, 795, 108
Staveley-Smith L., Kim S., Putman M., Stanimirović S., 1998, Rev. Mod. Astron., 11, 117
Stetson P. B., 1987, PASP, 99, 191
Tandon S. N. et al., 2020, AJ, 159, 158
Udalski A., Szymański M. K., Szymański G., 2015, AcA, 65, 1
Virtanen P. et al., 2020, Nature Methods, 17, 261
Zivick P. et al., 2019, ApJ, 874, 78

SUPPORTING INFORMATION

Supplementary data are available at *MNRAS* online.

FUV-catalog-cluster.zip

Please note: Oxford University Press is not responsible for the content or functionality of any supporting materials supplied by the authors. Any queries (other than missing material) should be directed to the corresponding author for the article.

APPENDIX A: STELLAR PARAMETERS OF HOT MS TURN-OFF STARS IN CLUSTERS

Table A1. Hot MS stars in clusters of Tile 1: BS 245 ($D = 56$ kpc, $A_V = 0.49$ mag), OGLE-MBR-CL-0084 ($D = 50$ kpc, $A_V = 0.19$ mag), and OGLE-MBR-CL-0030 ($D = 50$ kpc, $A_V = 0.41$ mag).

Object	RA (deg)	Dec (deg)	$T_{\rm eff}$ (K)	log g	$Z/Z_{\odot}$	χ^2	$eT_{\rm eff}$ (K)	$e\log g$	*Vgfb*
4643350377055618048	36.85	−73.98	42500	4.0	0.2	225.01	1250	0.12	2.65
4643350411415356800	36.89	−73.98	37500	3.75	0.2	312.37	1250	0.12	2.33
4643350613278417152	36.87	−73.95	16000	2.5	0.2	9.55	500	0.15	1.82
4643350273976401792	36.78	−73.96	18000	2.25	0.2	30.26	500	0.12	0.89
4643446270789964544	37.07	−73.82	24000	2.75	0.2	120.95	500	0.12	1.51
4643446378164870912	37.10	−73.80	23000	2.5	0.2	151.03	500	0.12	1.28
4643446687401405952[a]	37.45	−73.81	18000	2	0.2	519.24	500	0.12	79.15

Note.[a] Due to the high Vgfb value, the estimated parameters are not reliable for this star.

Table A2. Hot MS stars in clusters of Tile 2: OGLE-MBR-CL-0070 ($D = 45$ kpc, $A_V = 0.41$ mag) and OGLE-MBR-CL-0026 ($D = 50$ kpc, $A_V = 0.41$ mag).

Object	RA (deg)	Dec (deg)	$T_{\rm eff}$ (K)	log g	$Z/Z_\odot$	χ^2	$eT_{\rm eff}$ (K)	$e\log g$	*Vgfb*
4637563265106068608	32.99	−74.12	18000	2.5	0.2	10.12	500	0.12	2.61
4637563475560490752	32.96	−74.12	32500	3.5	0.2	159.67	125	0.12	2.23
4637563475560492416	32.96	−74.12	23000	3.25	0.2	49.81	500	0.12	2.13
4637562376048872320	33.05	−74.17	26000	3.25	0.2	29.21	500	0.12	1.48
4637562376048872448	33.04	−74.17	24000	3.0	0.2	1222.84	500	0.12	11.29
4637562376048870784	33.04	−74.16	17000	2.25	0	24.47	500	0.12	2.45
4637562135529216000	33.04	−74.18	24000	3.0	0.2	40.33	500	0.12	1.80
4637562376048870528	33.07	−74.16	30000	3.25	0.2	24.8	1236	0.12	1.21
4637562135530803584	33.04	−74.19	32500	3.75	0.2	642.21	1250	0.12	5.55
4637562474831940992	33.12	−74.18	32500	3.5	0.2	49.99	1250	0.12	1.47
4637562238609919616	32.97	−74.18	29000	3.25	0.2	87.91	500	0.12	1.67
4637562444768446848	33.01	−74.15	23000	3.0	0.2	84.52	500	0.12	3.56

Table A3. Hot MS stars in clusters of Tile 3: OGLE-MBR-CL-0075 ($D = 44.7$ kpc, $A_V = 0.30$ mag).

Object	RA (deg)	Dec (deg)	$T_{\rm eff}$ (K)	log g	$Z/Z_\odot$	χ^2	$eT_{\rm eff}$ (K)	$e\log g$	*Vgfb*
4638262180841330688[a]	29.18	−74.219488	55000	4.5	0.2	345.98	1250	0.16	97.7
4638262180838395392	29.19	−74.22	18000	2.0	0.2	199.05	500	0.12	12.36
4638262176545884800	29.19	−74.22	16000	2.0	0	20.19	501	0.12	1.51
4638262176545986944	29.19	−74.22	17000	2.0	0.2	59.73	500	0.12	3.21
4638262249559947520	29.16	−74.21	15000	2.0	0.2	194.85	500	0.12	2.32
4638261970387444352	29.21	−74.23	21000	2.25	0.2	456.15	500	0.12	6.06

Note.[a] Due to the high Vgfb value, the estimated parameters are not reliable for this star.

Table A4. Hot MS stars in clusters of Tile 4: L 114 ($D = 44.7$ kpc, $A_V = 0.41$ mag).

Object	RA	Dec.	$T_{\rm eff}$	log g	$Z/Z_\odot$	χ^2	$eT_{\rm eff}$	$e\log g$	*Vgfb*
4638268296872116864[a]	27.577465	−74.356262	18000	2.0	0	400.3	958	0.12	97.48
4638268296874014592	27.584589	−74.353194	20000	2.25	0.2	78.98	500	0.12	5.09
4638268292577898368	27.570701	−74.358473	24000	2.5	0.2	187.31	500	0.12	4.72
4638268223858422528	27.596802	−74.354399	18000	2.25	0.2	25.78	500	0.12	2.47
4638268296874017408	27.564135	−74.359202	18000	2.0	0.2	70.11	500	0.12	1.49
4638268292577898752	27.559396	−74.357764	20000	2.25	0	41.07	500	0.12	1.83
4638268223858422144	27.602234	−74.35802	18000	2.0	0.2	84.9	500	0.12	1.69
4638268292577904000	27.58081	−74.348271	22000	2.5	0.2	33.98	500	0.12	1.55
4638268228154541312	27.606952	−74.359972	18000	2.0	0.2	28.72	502	0.12	1.23
4638268223858423680	27.604314	−74.350515	21000	2.5	0.2	69.1	500	0.12	1.65
4638268223858409472	27.6078	−74.362732	18000	2.5	0.2	29.0	500	0.12	2.49
4638268945412931840	27.532019	−74.351616	15000	1.75	0	8.79	500	0.12	1.72
4638269048492149632	27.537347	−74.347878	18000	2.25	0.2	26.41	500	0.12	1.27
4638268326938392832	27.616212	−74.345966	16000	2.0	0.2	26.42	500	0.12	11.3
4638268193794800384	27.519284	−74.355946	20000	2.5	0.2	40.14	500	0.12	1.79
4638268120779185920	27.57279	−74.372479	16000	2.0	0.2	20.73	500	0.12	2.36
4638268052059716608	27.638503	−74.361964	16000	2.25	0.2	26.58	500	0.12	1.98
4638269052788256000	27.5337	−74.340586	21000	2.75	0.2	70.71	500	0.12	1.44
4638267914620753152	27.580858	−74.375913	15000	2.25	0.2	17.93	500	0.13	4.5
4638268120779182464	27.559693	−74.377115	15000	2.25	0.2	14.09	502	0.17	1.01
4638268189498665984	27.516457	−74.372157	21000	2.5	0.2	40.02	500	0.12	0.96
4638268155138933120	27.503633	−74.368156	15000	2.5	0.2	11.42	500	0.2	2.47
4638268125075330816	27.54377	−74.380597	20000	2.75	0.2	121.98	500	0.12	1.8
4638267914620745472	27.576373	−74.384191	15000	2.0	0.2	19.42	500	0.12	3.81
4638268086419443200	27.517562	−74.380762	15000	1.75	0.2	10.69	500	0.12	4.75
4638267987636374144	27.691262	−74.364093	21000	2.75	0.2	71.84	500	0.12	2.72

Note.[a] Due to the high Vgfb value, the estimated parameters are not reliable for this star.

APPENDIX B: CLUSTER MEMBERSHIP, KDE, AND SPATIAL PLOTS

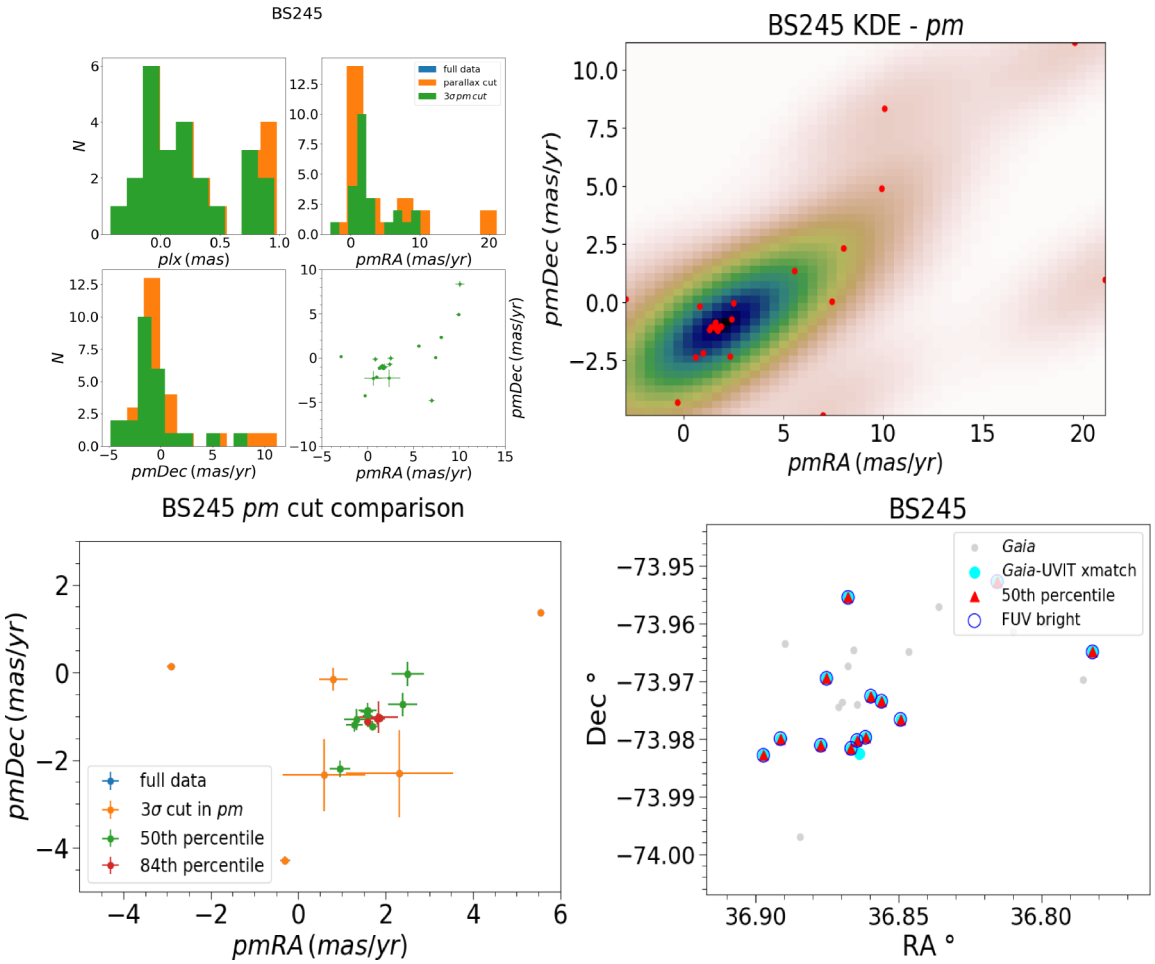

Figure B1. BS245.Top left: Distribution of stars after preliminary cuts in parallax and pm. The panel description is as in Fig. 4. Top right, bottom left, bottom right: KDE analysis, 2D pm percentile cut, spatial plot. The panel description is as in Fig. 5.

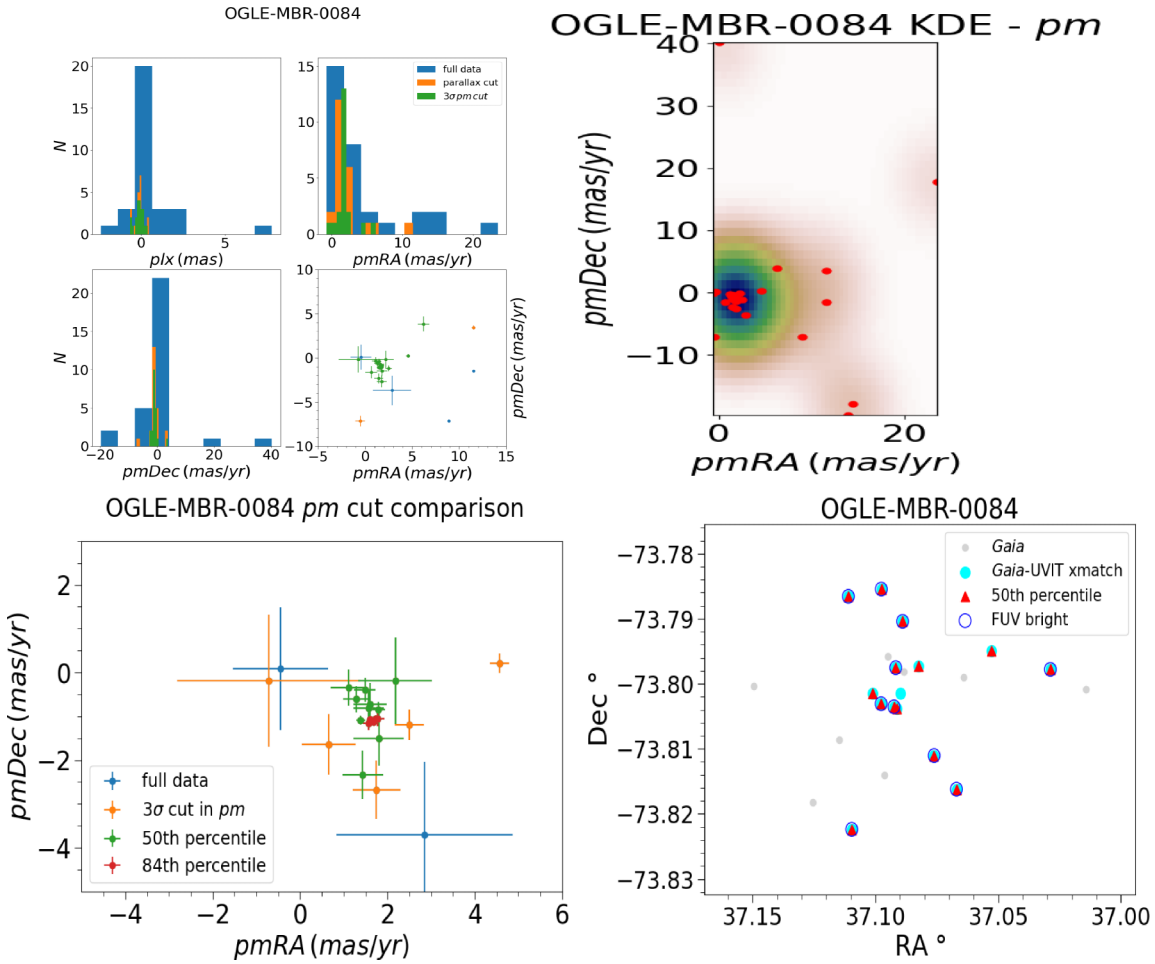

Figure B2. As Fig. B2 but for OGLE-MBR-CL-0084.

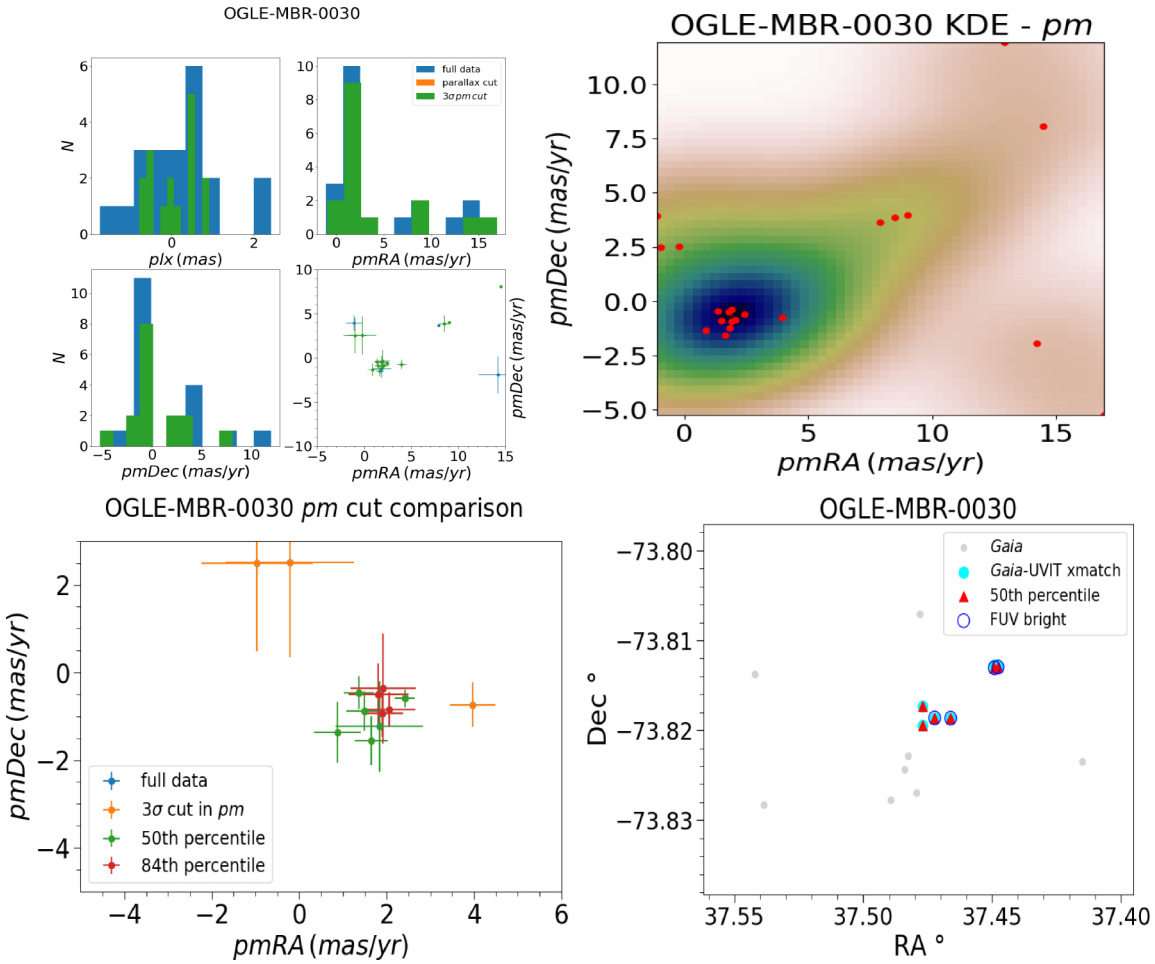

Figure B3. As Fig. B2 but for OGLE-MBR-CL-0030.

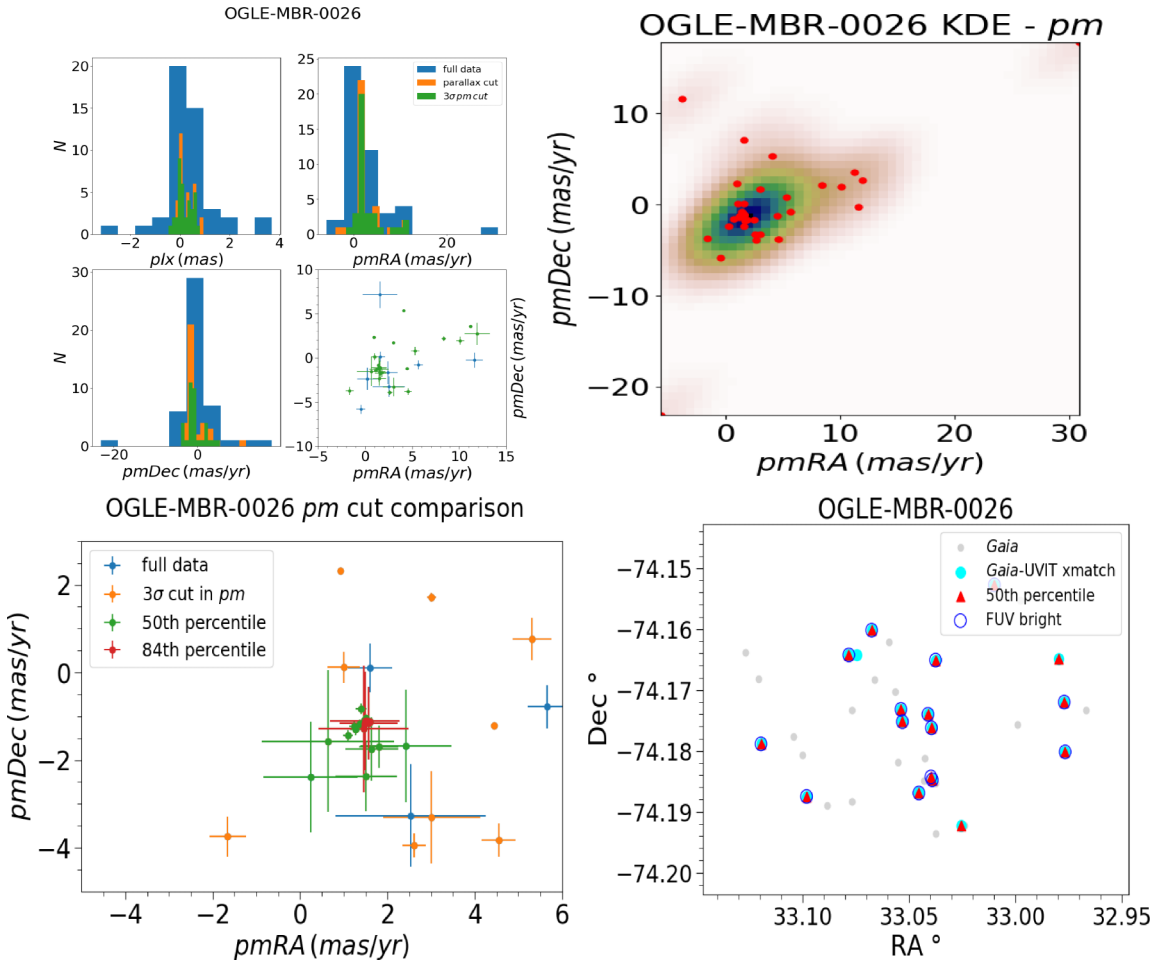

Figure B4. As Fig. B2 but for OGLE-MBR-CL-0026.

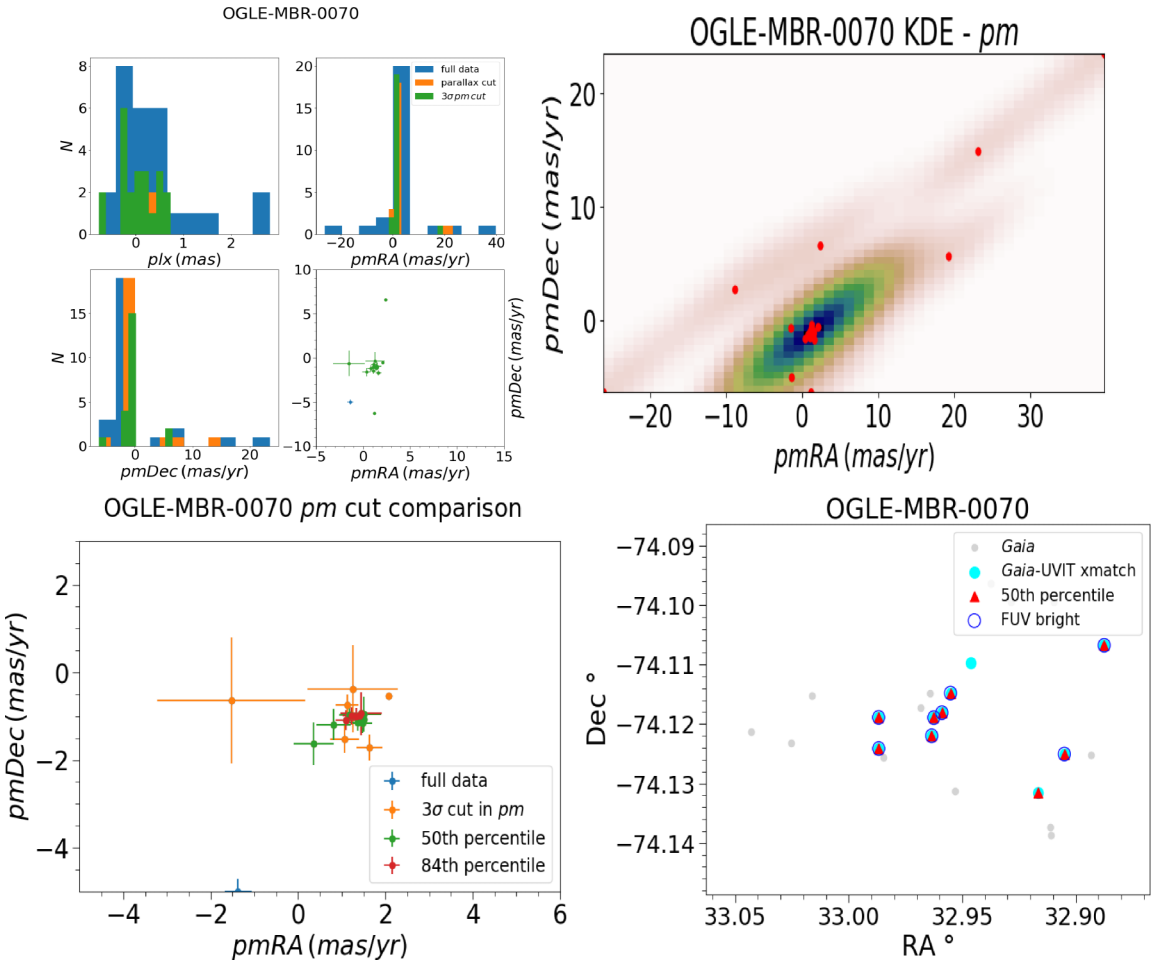

Figure B5. As Fig. B2 but for OGLE-MBR-CL-0070.

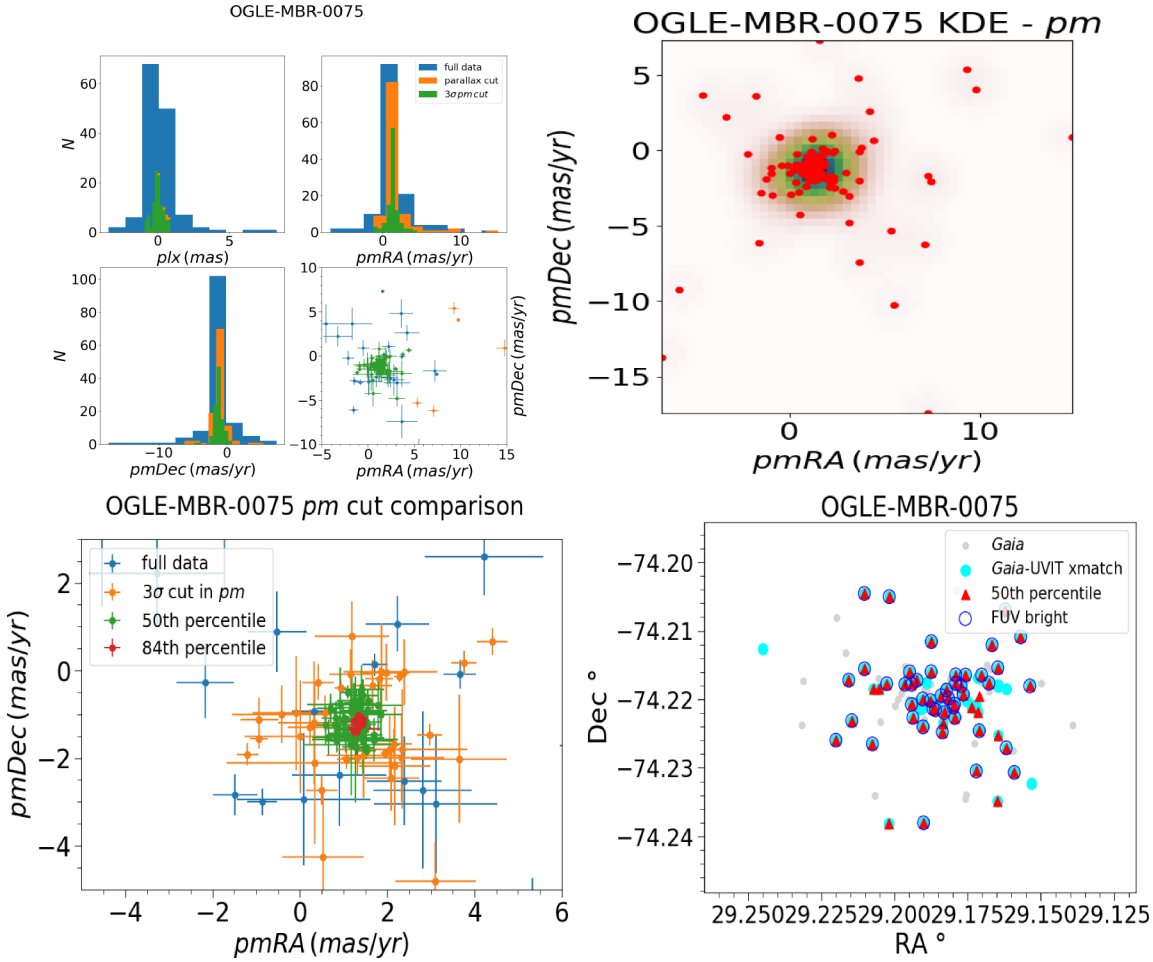

Figure B6. As Fig. B2 but for OGLE-MBR-CL-0075.

APPENDIX C: SPECTRAL ENERGY DISTRIBUTION OF ALL HOT MS STARS IN CLUSTERS

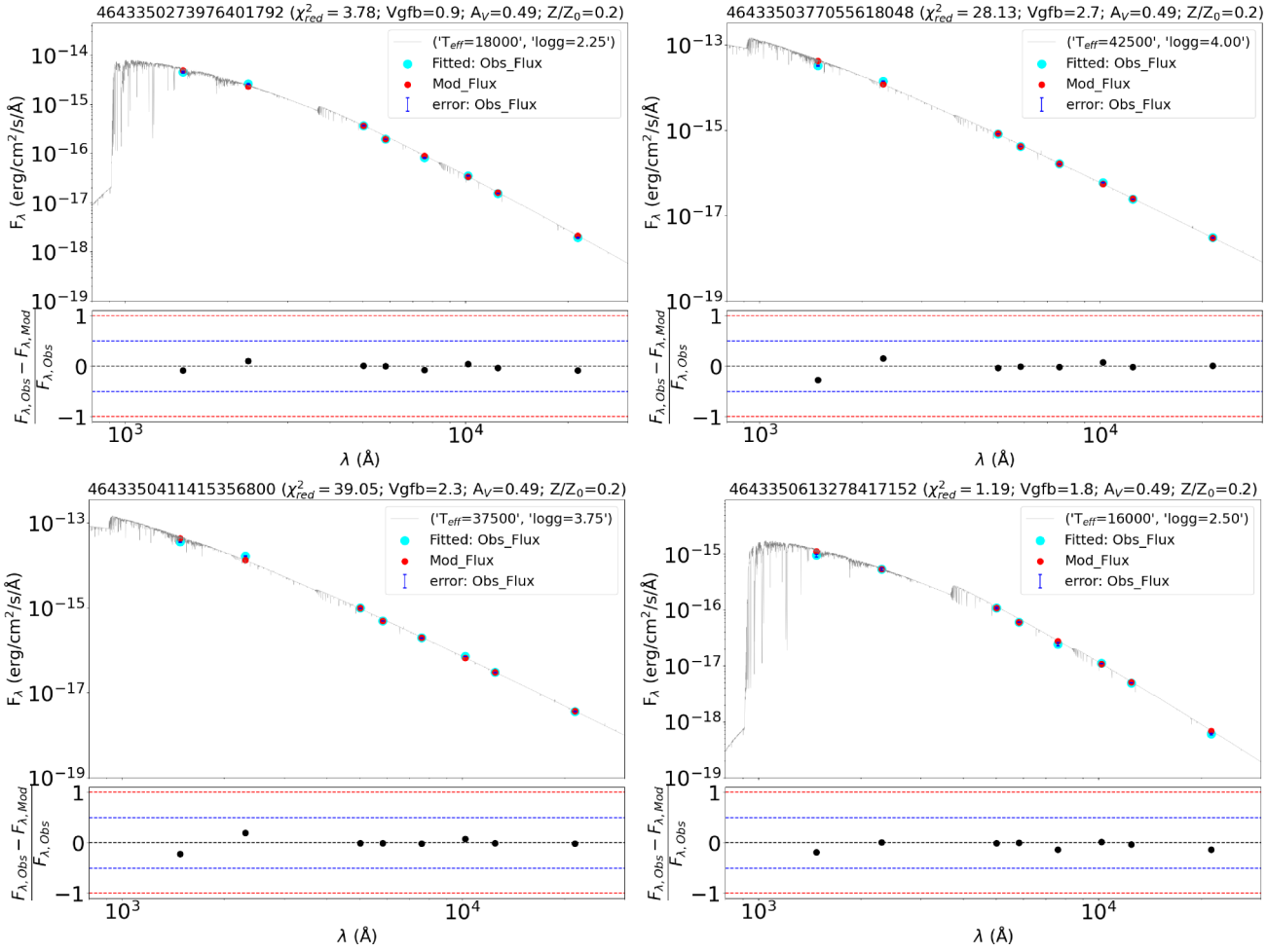

Figure C1. SED of MS stars in BS 245 (Tile 1); description as for Fig. 10.

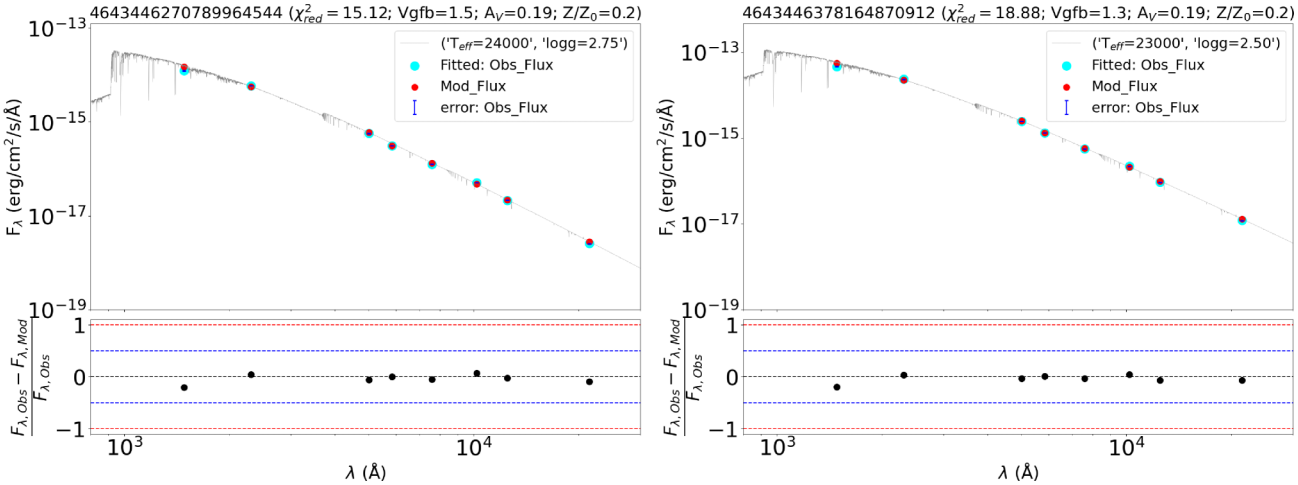

Figure C2. As Fig. C1 but for OGLE-MBR-CL-0084 (Tile 1).

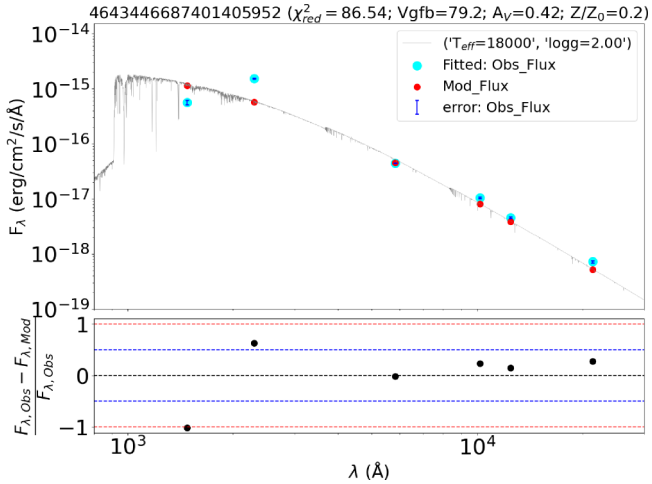

Figure C3. As Fig. C1 but for OGLE-MBR-CL-0030 (Tile 1).

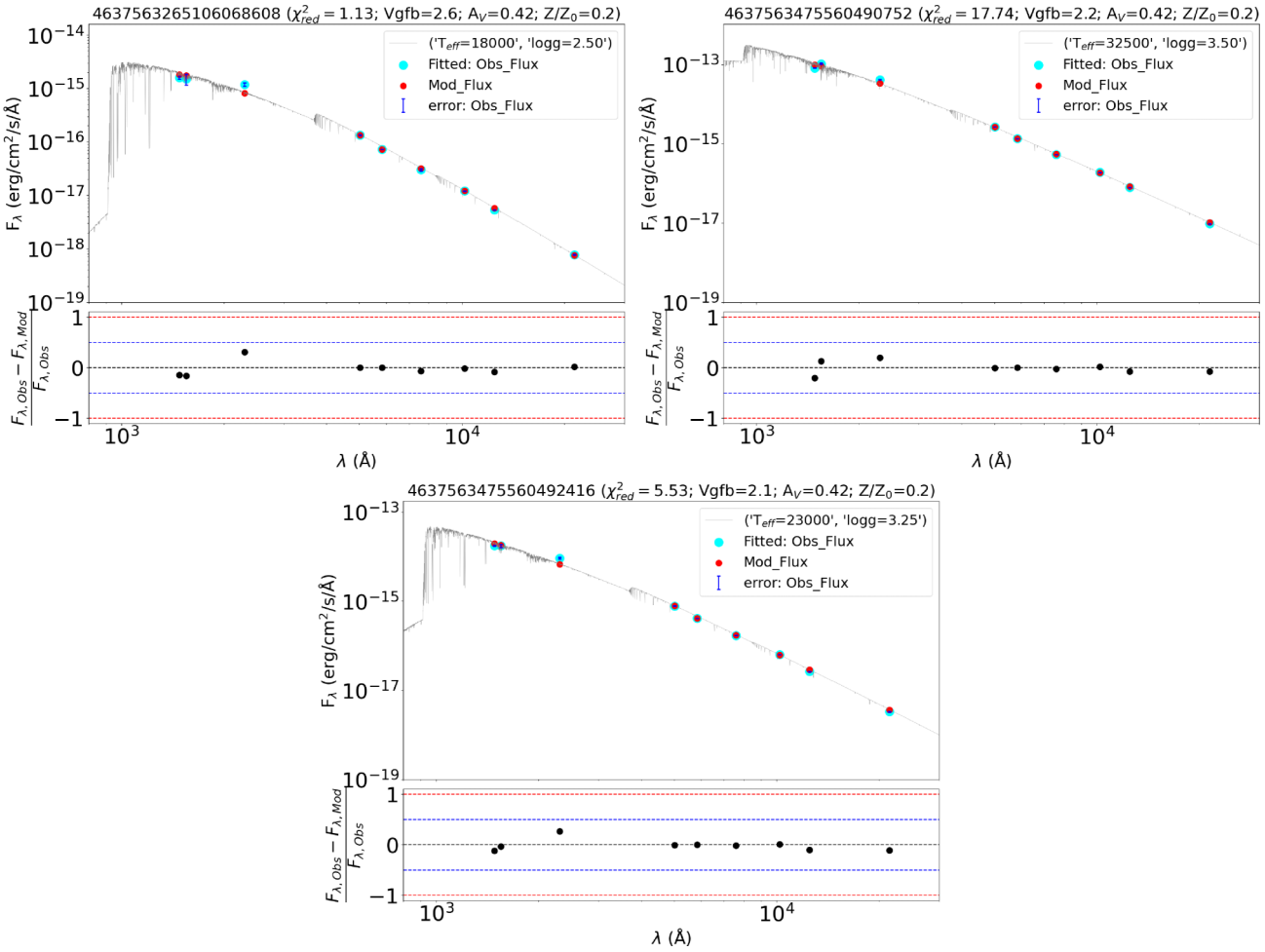

Figure C4. As Fig. C1 but for OGLE-MBR-CL-0070 (Tile 2).

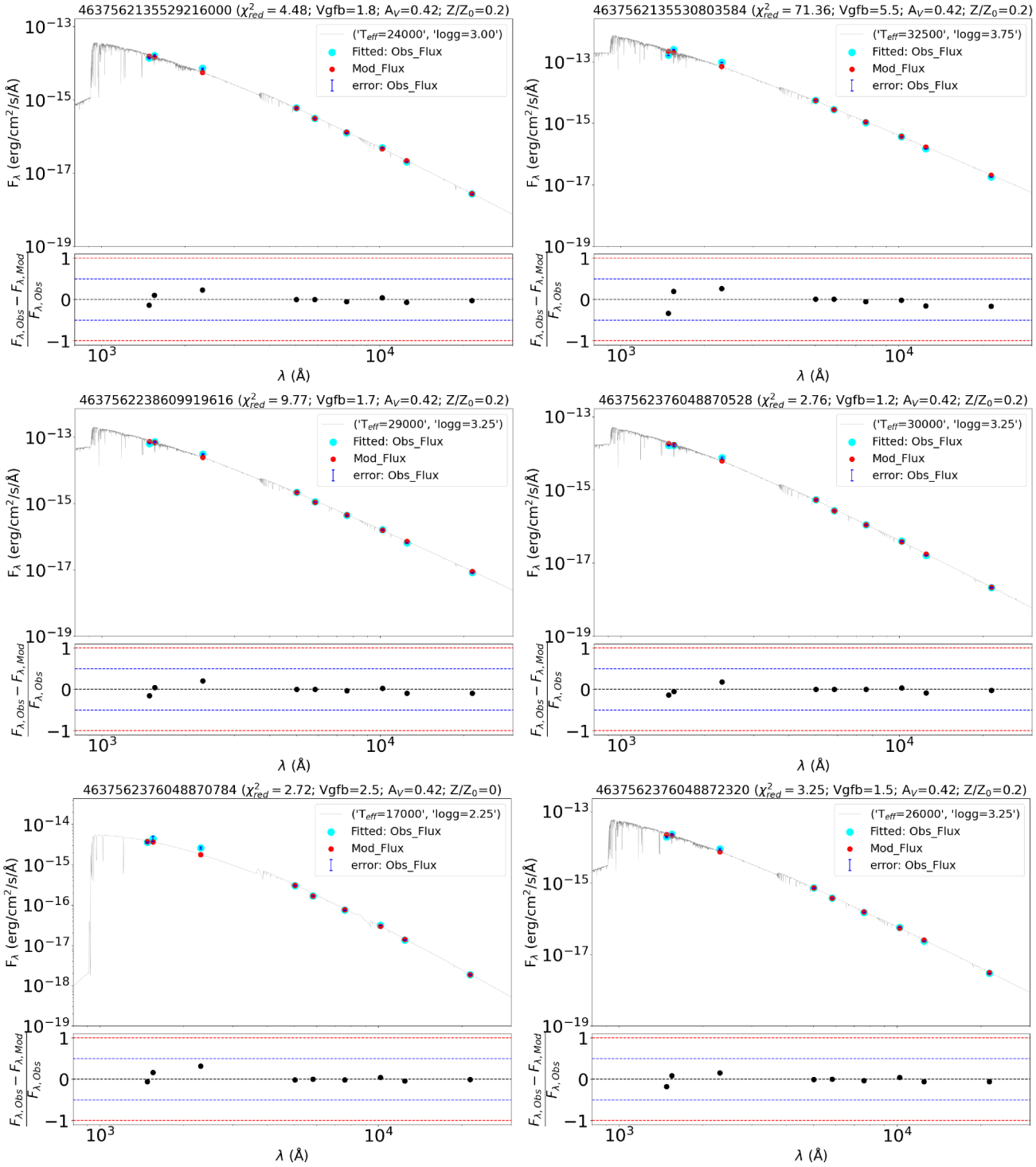

Figure C5. As Fig. C1 but for OGLE-MBR-CL-0026 (Tile 2).

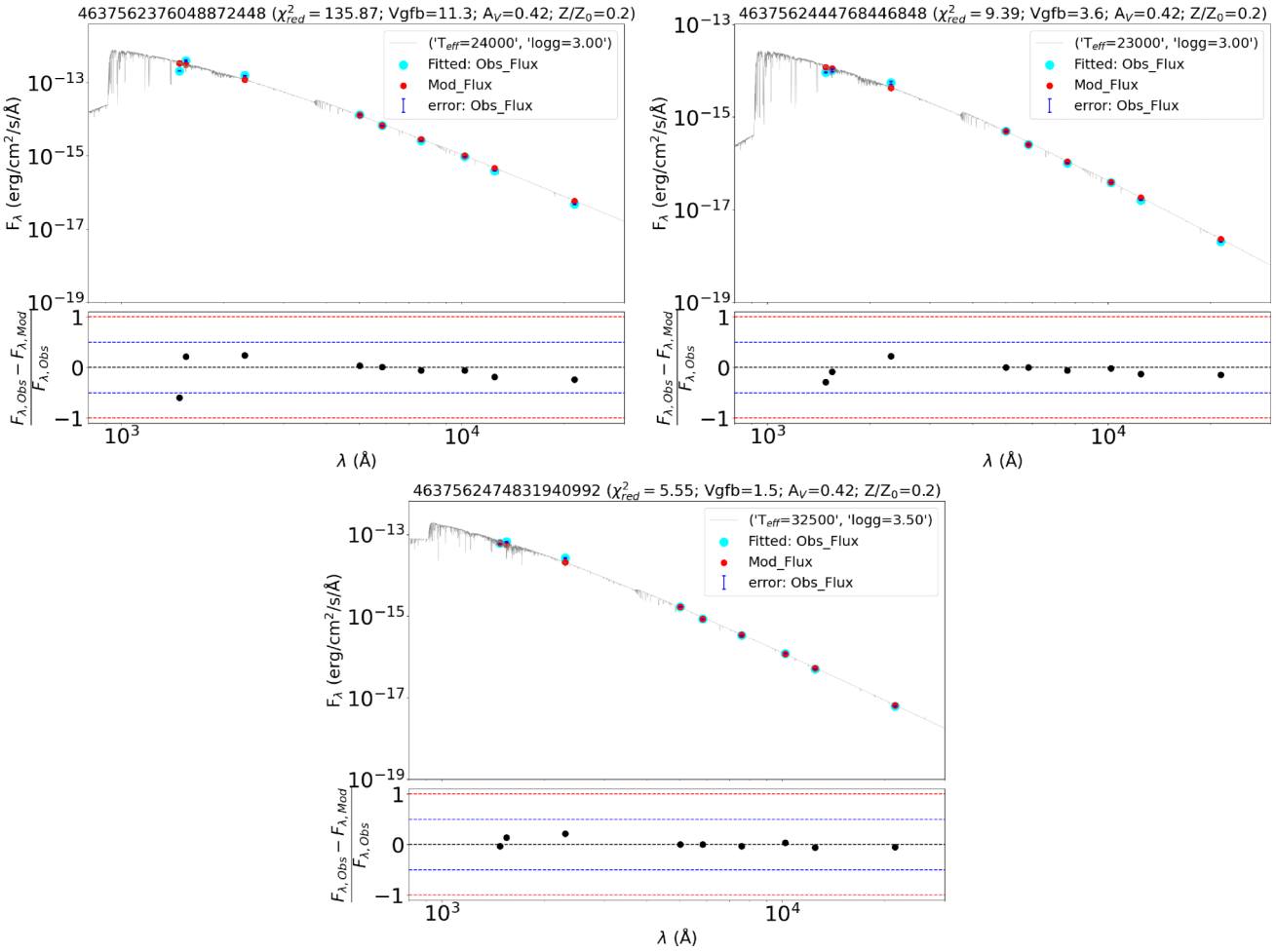

Figure C6. Continued from Fig. C5.

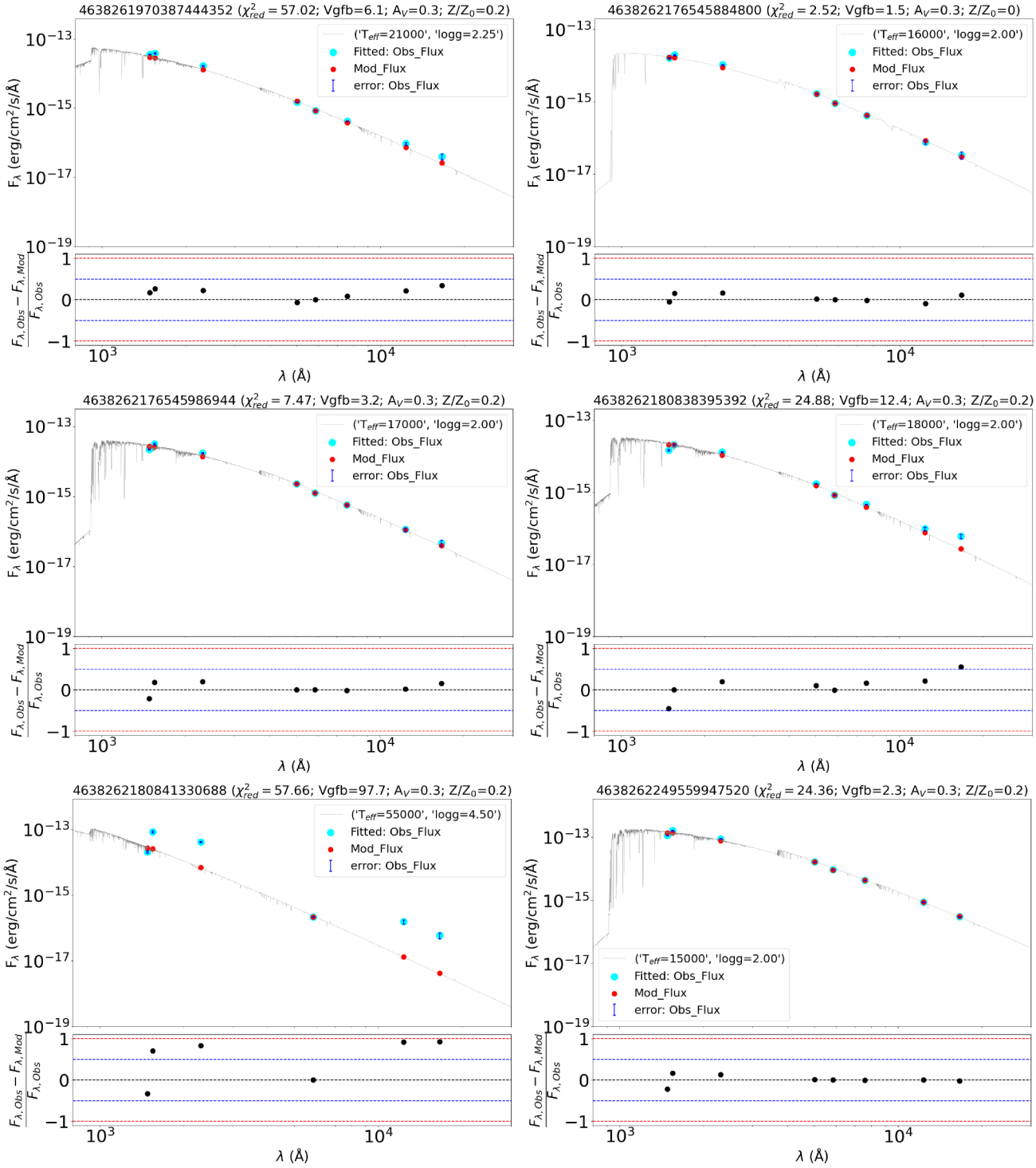

Figure C7. As Fig. C1 but for OGLE-MBR-CL-0075 (Tile 3).

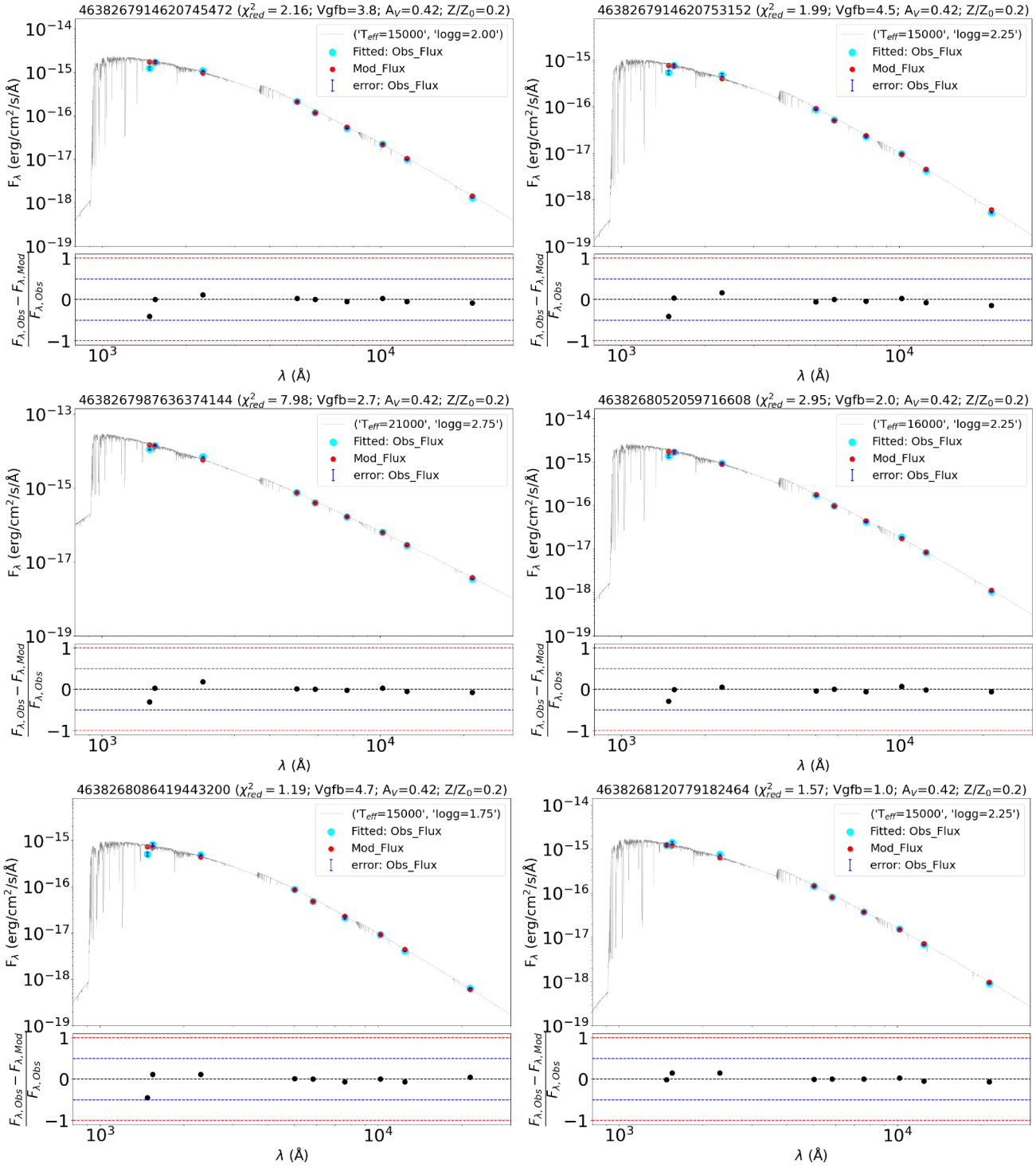

Figure C8. As Fig. C1 but for L 114 (Tile 4).

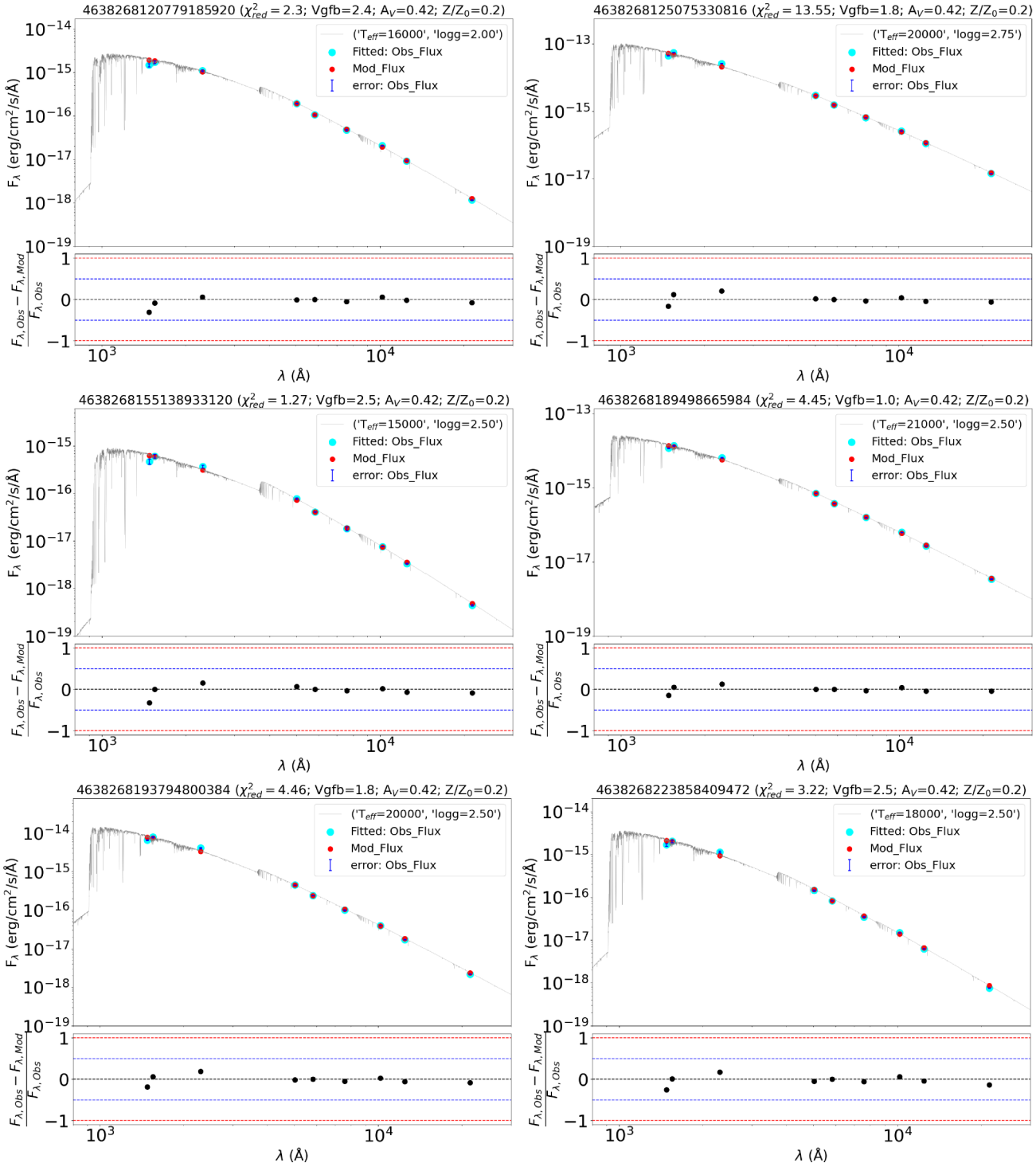

Figure C9. Continued from Fig. C8.

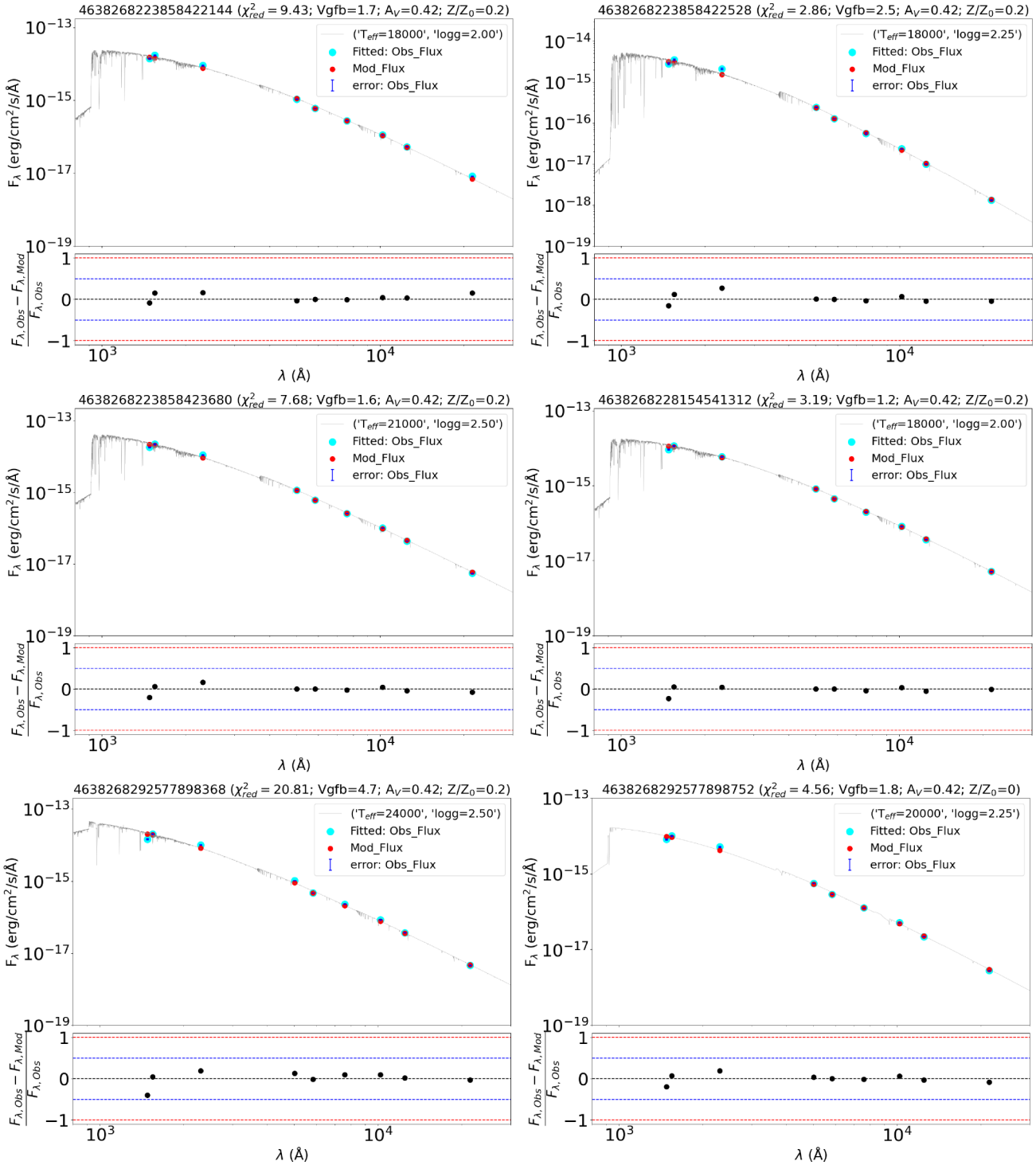

Figure C10. Continued from Fig. C8.

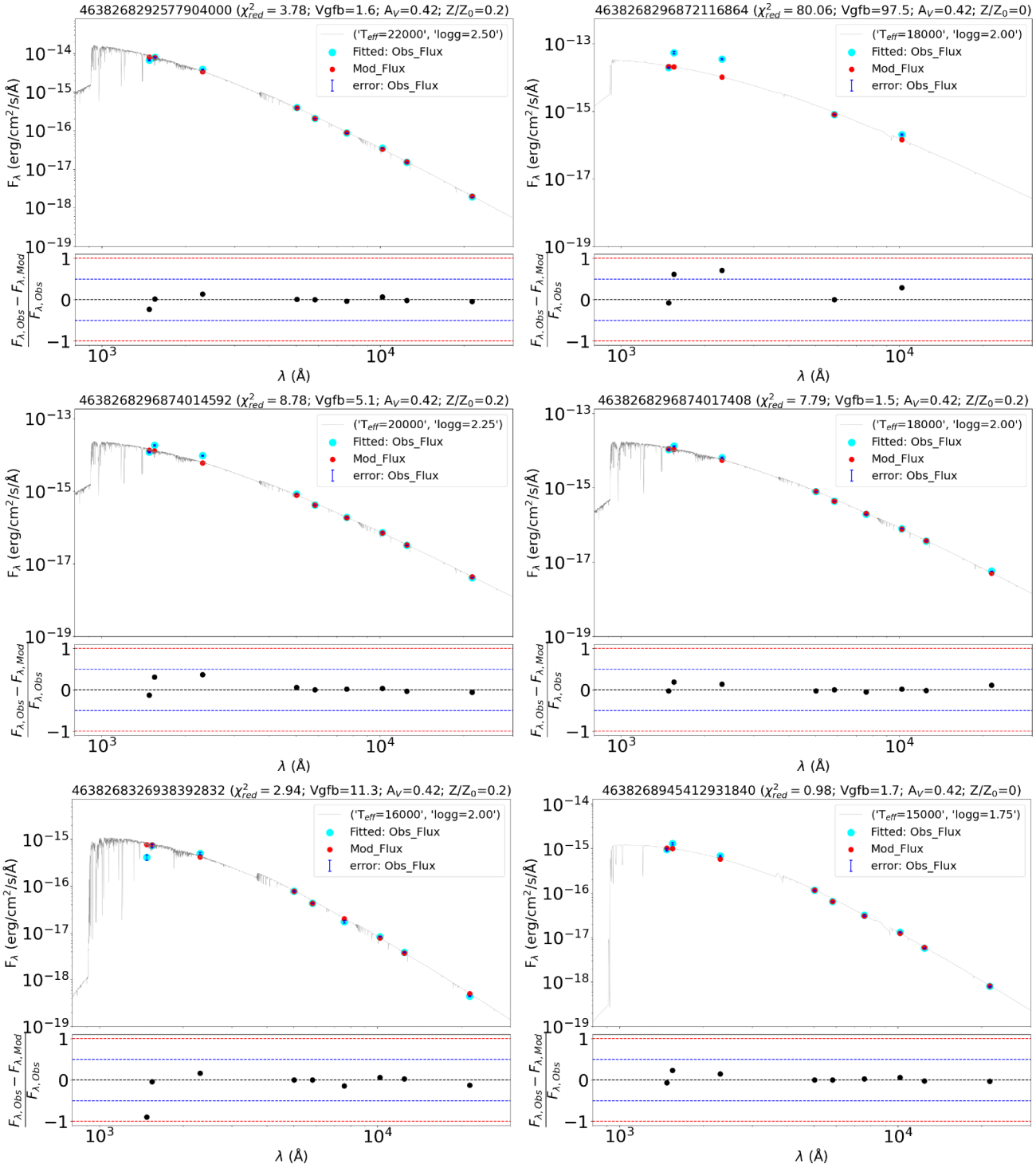

Figure C11. Continued from Fig. C8.

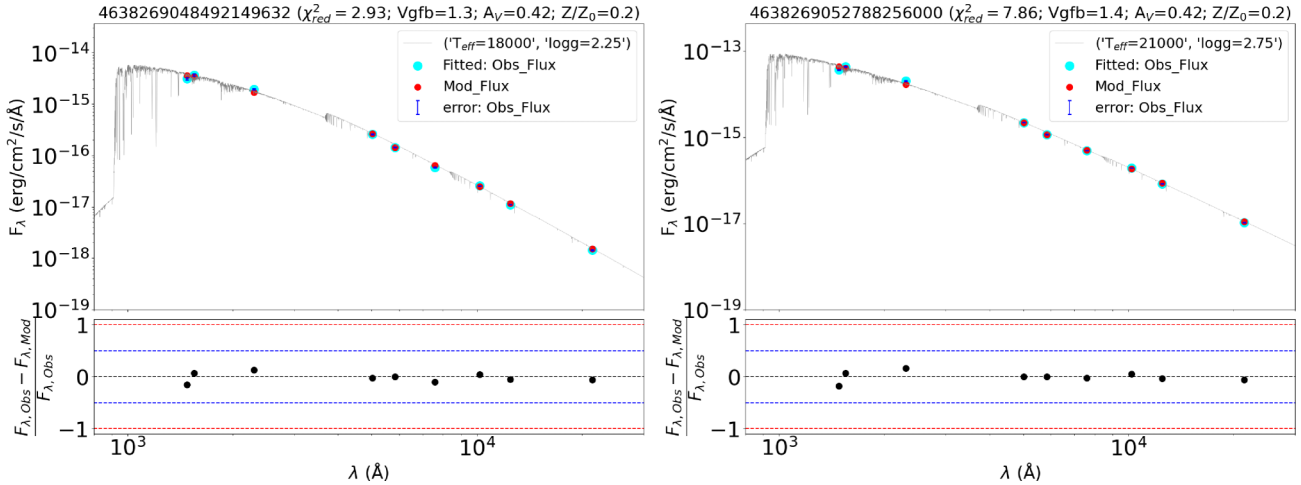

Figure C12. Continued from Fig. C8.

This paper has been typeset from a TEX/LATEX file prepared by the author.